The inductively coupled R.F. (radio frequency) plasma

Maher I. Boulos

Chemical Engineering Department, Université de Sherbrooke,
Sherbrooke, J1K 2R1, Québec, Canada

Abstract - A review is made of the basic principals and the main de-
sign features of the inductively coupled radio frequency (r.f.) plas-
ma.   Special attention is given to diagnostic measurements carried
out by different investigators in order to determine the charasteris-
tics of the electric and magnetic fields, the temperature, velocity
and concentration distributions in the discharge region. Mathematical
modelling is discussed giving an overview of the different models
proposed and typical results obtained. Applications of the inductive-
ly coupled plasma technology in material processing, synthesis of
ultra fine powders and spectrochemical elemental analysis are briefly
reviewed.

INTRODUCTION

While the first experiments on low-pressure electrodless discharges can be traced back to
the end of the nineteenth century, the atmospheric pressure induction discharge was only
discovered in the fourties. In 1947, Babat (ref. 1) was the first to report that a ring
discharge, once established at low pressure, can be maintained, while the pressure is
raised up to atmospheric pressure.

The next major development which lead to the induction plasma as we know it today, is that
due to Reed (ref. 2) in 1961. Reed's principal contribution was to show that an inductive-
ly coupled plasma discharge can be maintained in an open tube in the presence of a stream-
ing gas. Upon leaving the discharge region, the partially ionized gas forms a low veloci-
ty plasma jet with an average temperature in the range of 8000 to 10000 K. Interestingly
enough, inspite of the numerous investigations reported over the last twenty years, the
basic design of the inductively coupled plasma torch hardly changed compared to that ori-
ginally published by Reed.

Considerable progress, however, thas been achieved in our understanding of the characte-
ristics of such an important plasma generating device and its principal design and opera-
tion parameters. An excellent review on the subject has been published by Eckert (ref. 3)
in 1974.

In this paper, a brief review will be made of the basic principals and the main design
features of the inductively coupled plasma. This will be followed by a discussion of
diagnostic measurements carried out by different investigators in order to determine the
characteristics of the electric and magnetic fields, the temperature, velocity and concen-
tration fields in the discharge region. Mathematical modelling will be discussed next,
giving an overview of the different models proposed and typical results obtained. Finally,
applications of the inductively coupled plasma technology in such areas as material pro-
cessing, synthesis of fine powders and spectrochemical elemental analysis will be discus-
sed.

1-COUPLING MECHANISM

The basic phenomena governing the operation of inductively-coupled plasmas, Fig. 1, are
essentially similar to that of the induction heating of metals which has been known since
the beginning of the century and has found numerous large scale industrial applications
over the last fourty years (ref. 4).

With induction plasmas, howver, the fact that the "load" is the conducting plasma gas
with a substantially lower electrical conductivity than most metals, has a direct influen-
ce on the optimal frequency, size and power combination necessary to sustain a stable
discharge. The coupling mechanism is best demonstrated by the relatively simple channel
model developed by Freeman and Chase (ref. 5) in 1968 based on a close analogy with the
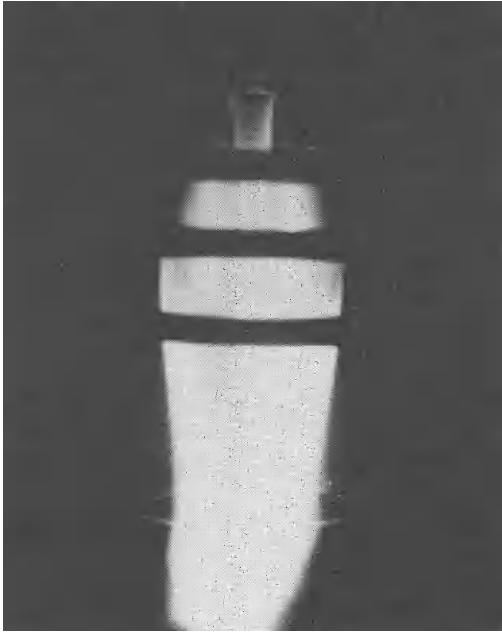induction heating of metals.

Fig. 1. An inductively coupled r.f.
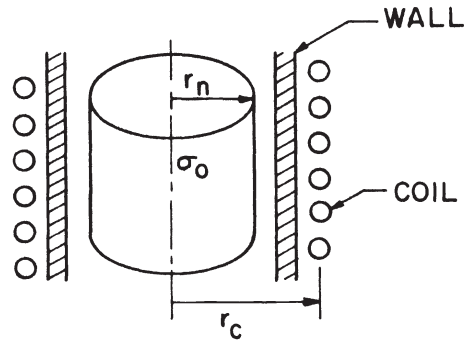plasma in the presence of strong
central injection.

Fig. 2. Schematic of the channel model
(after Freeman and Chase (ref. 5)).

According to this model, the current-carrying plasma in the coil region can be represent-
ed, as shown in Fig. 2, by an equivalent cylindrical work load of radius, r_n, and uni-
form temperature and electrical conductivity. Outside this region, the gas is assumed to
be non-conducting, and spans the temperature difference between that of the plasma and the
wall of the plasma confinement tube.

1.1-Skin Depth and Coupling Efficiency

Based on conventional induction heating theory, the application of an oscillating magnetic
field results in the generation of eddy currents in the external cylindrical shell of the
load. The thickness of this shell, generally known as the skin depth, δ, is a function of
the oscillator frequency, f, and the average electrical conductivity of the load, σ. It
can be estimated as,

$$\delta = \left[\frac{1}{\pi \, \xi_0 \, \sigma \, f} \right]^{\frac{1}{2}} \tag{1}$$

Where ξ_0, is the magnetic permeability of the load which may be taken for a plasma, as
that for free space $\xi_0 = 4\pi \times 10^{-7}$ Hy/m.

For an induction plasma operating with argon at atmospheric pressure with an average tem-
perature of 8000 K, $\sigma = 10^3$ mhos/m. The skin depth would be about 8 mm for an oscillator
frequency of 4 MHz. A reduction of the oscillator frequency would result in an increase
of the skin depth, and a more uniform distribution of the energy dissipation in the plas-
ma. The effect was observed by Thorpe and Scammon (ref. 6) looking at an end view of the
discharge.

An analysis of the variation of the coupling efficiency, η_c, as a function of the ratio
of the plasma radius to the skin depth (r_n/δ) has been reported by Eckert (ref. 7) and
by Mensing and Boedeker (ref. 8). The results shown in Fig. 3, for an argon plasma at
atmospheric pressure indicate the coupling efficiency, defined as the ratio of the dis-
charge power to the reactive power, is a function of the coupling parameter $(\kappa = \sqrt{2} \, r_n/\delta)$,
with the ratio of the plasma radius to that of the coil (r_n/r_c) as a parameter.

It may be noted that optimum coupling, denoted by the dashed line in Fig. 3, is obtained
for values of (r_n/δ) between 1.5 and 4.0 depending on the value of (r_n/r_c). At the
higher values of (r_n/δ), the energy dissipation is limited to a rather thin shell around
the discharge with a gradual loss in coupling efficiency. On the other hand, at very low
values of (r_n/δ), less than 1.0, the coupling efficiency drops rather drastically.

As noted in Fig. 3, the coupling efficiency for an induction plasma also depends to a large extent on the ratio of the plasma radius to that of the induction coil. A ratio of (r_n/r_c) as close as possible to 1.0 is most desirable, although because of mechanical constraints, values of approximately 0.7 to 0.8 for this parameter are still quite acceptable.

One way of improving the ratio (r_n/r_c), and accordingly the coupling efficiency, is by scaling-up. The larger the plasma diameter, the closer will be the ratio (r_n/r_c) to unity. An increase of r_n, however, has to be accompanied by a decrease in the operating frequency and an increase in the power level.

Fig. 4, gives the ideal coupling efficiency, (obtained with a tight discharge i.e. (r_n/r_c) = 1.0), as function of the plasma diameter and the operating frequency. Good coupling can be obtained with plasmas operating with a frequency as low as 960 Hz or even 60 Hz. The plasma diameter and accordingly the operating power, however, have to be sufficiently large to sustain the discharge.
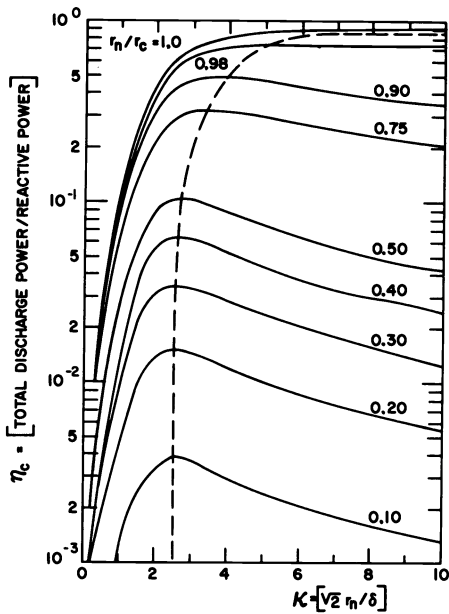

Fig. 3. Coupling efficiency as function of the coupling parameter (after Mensing and Boedeker (ref. 8)).
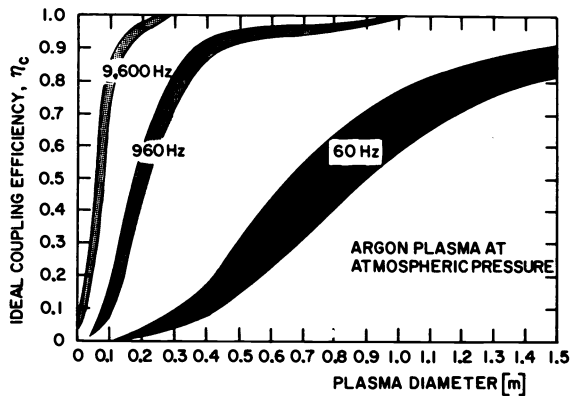

Fig. 4. Ideal coupling efficiency as function of the plasma diameter and the operating frequency (after Vogel et al. (ref. 9)).

1.2-Minimum sustaining power

An estimate of the minimum power required to sustain a plasma under different operating conditions can be obtained from Fig. 5 (after Pool et al. (ref. 10)).

It may be noted that for the operation of an induction torch with argon at atmospheric presure at a frequency of 960 Hz, the minimum sustaining power is close to 1 MW. The corresponding figure for 60 Hz operation would be more than 10 MW.

Fig. 5 shows that for a given oscillator frequency, the minimum sustaining power increases with the operating pressure and can change substantially with the gas composition. Since the minimum power requirement is lowest when operating with argon, it has become common practice to initiate the discharge with argon, then to switch gradually to the other gas while increasing the power level of the torch to avoid extinction of the plasma.
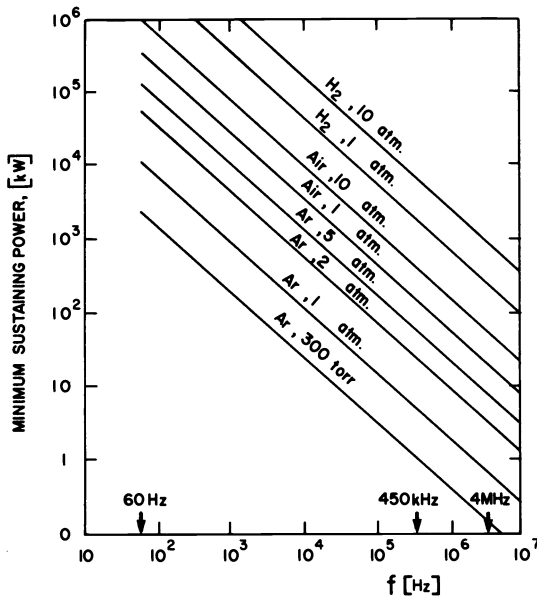
Fig. 5. Minimum sustaining power for
   an induction plasma
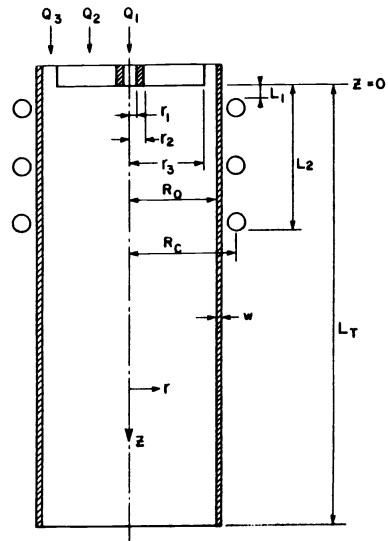   (after Pool et al. (ref. 10)).

Fig. 6. Schematic diagram of an
   inductively coupled plasma torch.

1.3-Torch design

A number of induction plasma torch designs have been developed and tested over the last
two decades. These varied widely in their power range (0.5 kW to almost 1.0 MW), opera-
ting frequency (9.6 kHz-40MHz) and mechanical construction.

Their basic design concept, however, has hardly changed as compared to that used by Reed
(ref. 2) in 1961. A schematic of a typical induction plasma torch is shown on Fig. 6.
This consists essentially of two concentric tubes with a small annular gap between them.
The outer tube, known as the plasma-confinement tube, is usually made of quartz and is
cooled on the outside by air or water, although transpiration cooling has also been used
(ref. 10).

In the discharge zone, the plasma confined tube is surrounded by a short, water-cooled,
copper induction coil, which normally consist of three or four turns. Their exact number
of turns depends on the electrical characteristics of the r.f. power supply.

The intermediate tube, which could be made of either quartz or a water-cooled segmented
metal sheath extends normally down to the level of the first turn of the induction coil.
It essentially serves to achieve a flow pattern in the torch with a relatively high velo-
city sheath gas, Q_3, flowing close to the inside wall of the plasma confinement tube in
order to reduce heat losses and to protect it from overheating.

Two other gas streams are also introduced in the torch. The central gas, Q_2, and the pow-
der or aerosol carrier gas, Q_1.

The central gas, sometimes known as the plasma gas is introduced inside the intermediate
tube and can include both swirl and axial velocity components. This gas serves essential-
ly to keep the plasma away from the intermediate tube. It also represents the main gas
component in which the discharge is taking place. Obviously there is a certain degree of
mixing between the central and the sheath gas streams.

Whenever applicable, the powder gas, or the aerosol carrier gas, Q_1, is generally introdu-
ced in the center of the discharge using a water-cooled probe the tip of which can be
maintained at the same level as the intermediate tube or made to penetrate further in the
discharge region.

In contrast to the air-cooled torches, the water-cooled induction torches are slightly more complicated in their mechanical construction but offers the principal advantage of being able to operate at much high power levels without the risk of damaging the plasma confinement tube.

Recently, two novel designs of the induction plasma torch have been reported. Of particular interest is the so-called "Hybrid Plasma" torch developed by Akashi and his collaborators (ref. 11) at the University of Tokyo which is characterized by the superposition of an r.f. plasma and a d.c. plasma jet. In spite of its obvious advantages in terms of plasma stability and the increased power density in the discharge, the added complication and cost of the electrical circuits necessary for the simultaneous operation of both d.c. and r.f. power supplies might hinder wider applications of such a device. Moreover, the presence of a d.c. plasma torch in the system can be a source of contamination of the plasma atmosphere through normal electrode errosion and would limit its use to applications where a high level of purity of the discharge is not required.

At Los Alamos National Labs (ref. 12) a new high-temperature plasma tube has been developed in order to overcome possible meltdown problems of conventional gas and water-cooled quartz plasma tubes commonly used. The key feature of this system in the placement of several heavy-walled, water-cooled, copper fingers indide a quartz mantle to sheald the mantle from the intense radiation of the plasma. The copper fingers also act as transformers to couple the plasma to the field of the coil. This design, however, has two serious limitations. The first is the lower energy transfer effeciency that is likely to be achieved by such an arrangement. Unfortunately no energy balance data is available. The second, is essentially a consequence of the presence of the copper fingers in direct contact with the plasma which could limit the use of such a torch to non-corrosive atmospheres. Its main advantages however, are the efficient protection of the quartz tube extending its life time almost indefinitely, and the ability to operate with considerably lower gas through puts than inductin plasma torches of conventional design.

1.4-Energy balance
In the design of any plasma generating device, one point of immediate concern is the overall energy utilization efficiency, η. This is defined as the ratio of the energy available as enthalpy in the plasma gas at the exit of the torch, to the electric energy supplied to the generator.

In contrast to d.c. torches which can be built to an overall energy efficiency of 60 to 80%, the efficiency of the inductively coupled plasma torches is typically in the range from 40 to 60%. The principal losses being in the radio- frequency generator, the coupling between the coil and the load, as well as energy transfered to the plasma-confinement tube.

A break-down of the losses in a typical r.f. induction plasma system is given in Fig.7. It is to be noted that the oscillator tube losses amount to almost constant and equal to 20% of the plate power while the transmission and coil losses, in this case, were only 9%. The torch coil losses, on the other hand, drops considerably with the increase in the ratio of (r_n/r_c) due to the improved electro-magnetic coupling, while the conduction, convection and radiation heat losses to the walls of the plasma confinement tube increases with the increase of the ratio of the plasma to the coil radius, due to the proximity of the plasma to the wall of the torch. An overall energy efficiency of approximately 50% can be achieved for a torch with a ratio of (r_n/r_c) of 0.7.

It should be noted, however, that the interpretation of the above values for the energy efficiency should be closely tied to the way in which the induction plasma torch is to be used. For example, would the torch be used as a gas heater with the materials to be processed injected in the tail flame at the exit of the torch, then an energy efficiency of approximately 50% is realistic. The situation is completely different in the event that the material to be processed is injected axially in the center of the discharge in the coil region. In this case better use will be made of the total energy dissipated in the plasma with the corresponding considerable increase of the effective energy efficiency to more than 70 or 80%. This is simply due to the fact that the torch wall losses should not be taken into account in this case in the overall energy balance.
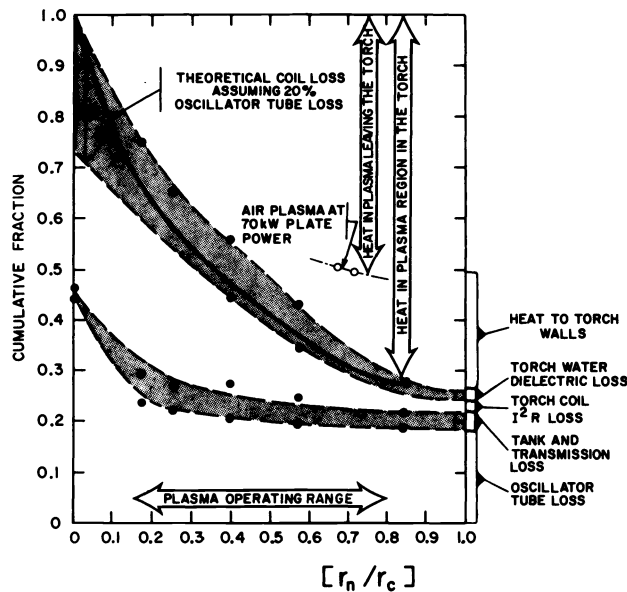
Fig. 7. Energy distribution in a typical induction plasma system
(after TAFA Eng. data Bull. 52-E5).

2-PRINCIPAL CHARACTERISTICS OF THE INDUCTIVELY COUPLED R.F. DISCHARGE

Considerable attention has been given to the determination of the characteristics of at-
mospheric pressure, inductively-coupled r.f. plasmas under different operating conditions.
The following parameters are of primary concern.

2.1-Electric and Magnetic Fields

Measurements of the magnetic field intensity profiles were carried out using miniature
water-cooled probes (ref. 13). Non-cooled probes were also used under transient condi-
tions (ref. 14).

Typical radial profiles of the magnetic field intensity in the presence and absence of the
discharge at the mid-section of the induction coil are shown in Fig. 8. These were ob-
tained by Eckert (ref. 13) for a 155 mm i.d. induction plasma torch with argon at atmos-
pheric pressure as the plasma gas. The oscillator frequency was 2.6 MHz and the dissipa-
ted power was estimated at 25 kW.

As expected, the presence of the discharge results in a substantial reduction of the ma-
gnetic field intensity in the center of the coil due to the interaction between the ap-
plied magnetic field and that resulting from the induction currents in the discharge. A
similar effect is also revealed by the axial profiles of the magnetic field intensity
along the centerline of the torch as shown in Fig. 9, after Trekhow et al. (ref. 14). In
this case, measurements were made using a 26 mm i.d. torch operated with an oscillator
frequency of 9 MHz and a power level of 27 kW. Curve 1 corresponds to the case without
the plasma while curves 2 and 3 corespond to a discharge in air and argon, respectively.

A dual magnetic probe system was later used by Eckert (ref. 15) in an attempt to measure
both the magnitude and the phase angle of the magnetic field in the central region of the
discharge. The variations of these parameters across the torch were used to determine the
current density and the electrical conductivity of the plasma as shown in Fig. 10, under
essentially the same conditions as those reported earlier (ref. 13).

2.2-Temperature distributions

Measurements of the temperature distributions in an induction plasma were mostly carried
out using emission spectroscopy. Other techniques such as absorption spectroscopy and
doppler broadenning were also used by Johnson (ref. 16) and Kleinmann and Cajko (ref. 17)
respectively. Measurements using enthalpy probes were reported by Dresvin and Klubnikin
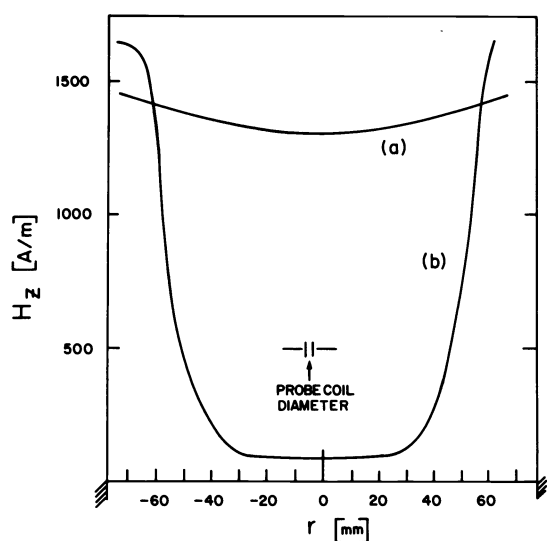(ref. 18).

Fig. 8. Radial profiles of the magnetic
field intensity at the mid-section of the
coil of an induction torch in the absence (a)
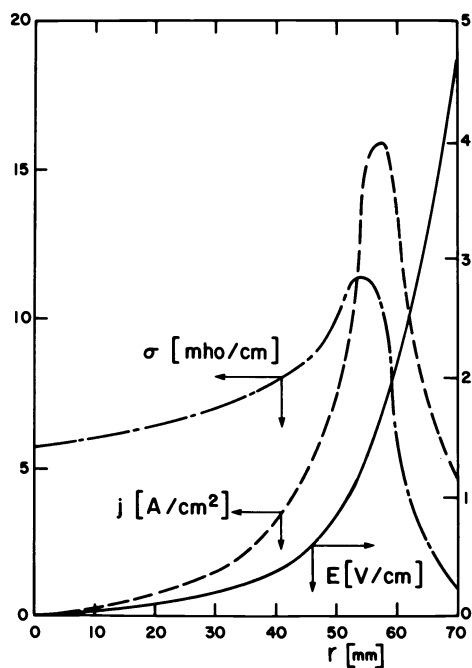and presence (b) of the discharge
(after Eckert (ref. 13)).

Fig. 10. Radial distribution of the
magnitude of the induced electric
field E , current density j and
electrical conductivity, σ, in an
argon induction discharge, f=2.6 MHz,
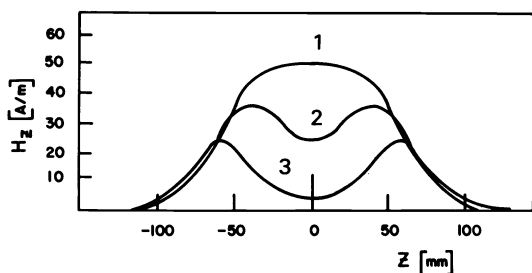P=25 kW (after Eckert (ref. 15)).

Fig. 9. Distribution of the magnetic field
intensity along the axis of the discharge
tube: (1) without plasma, (2) air plasma, (3)
argon plasma (after Trekhov et al. (ref. 14)).

Typical radial temperature profiles obtained by different investigators (ref. 19-23) at
the center of the coil region for an argon discharge at amospheric pressure are given in
Fig. 11, after Dresvin et al (ref. 24). These show an off-axis maximum temperature in the
range of 9500-10500 K. The fact that these profiles, while being axially symetric, do not
have their maximum on the centerline of the discharge can be directly attributed to the
skin effect. Since the energy dissipation in the discharge takes place essentially in the
outer annular shell of the plasma, the heating of the center of the discharge depends
primarily on conduction and convection transfer of heat from the external shell which
gives rise to lower temperatures observed in the center of the discharge. The difference,
however, while depending on the dimensions of the torch and the thickness of the skin
depth, are generally small and rarely exceed 1000 K.

A special attention was given to determine the effect of the plasma operating parameters
on the temperature field. Data compiled by Dresvin Ed (ref. 24) and given in Table 1
shows that for an argon plasma at atmospheric pressure, the maximum temperature of the
discharge is insensitive to the operating frequency but increases slightly with the in-
crease in the specific power dissipation, (P/V).

Table 1. Maximum plasma temperature for an induction
argon discharge as function of the specific power dissipation (P/V)
and the oscillator frequency (f). After Dresvin, Ed (ref. 24)

$(P_0/V) \times 10^6 \, kW/m^3$	f MHz	$T_{max} \times 10^3 \, K$
0.07	13	8.4
0.10	25	9.2
0.31	25	9.7
0.29	17	9.8
1.2	17	10.3
1.5	10	10.7

Goldfarb et al. (ref. 25,26) investigated the effect of the total plasma gas flow rate on
the temperature field at the exit of the torch. Data obtained for an argon plasma at
atmospheric pressure using a 14 mm i.d. plasma torch are shown in Fig. 12. The generator
used in this case had an oscillator frequency of 17 MHz and the plasma power was estimated
at 6-8 kW. It may be noted that the increase in the plasma gas flow rate gives rise to a
longer and slightly hotter flame which is attributed to the blowing of the hot core mate-
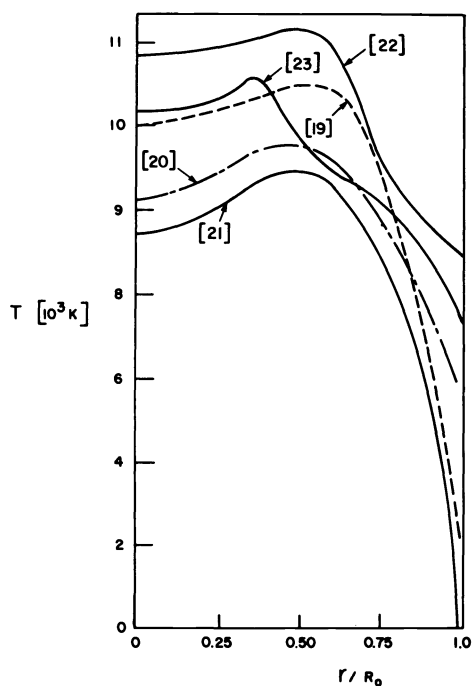rial from the inductor zone.

Fig. 11. Radial temperature profiles at the
mid-section of the inductin coil for an
argon plasma at atmospheric pressure.
Data obtained by different investigators
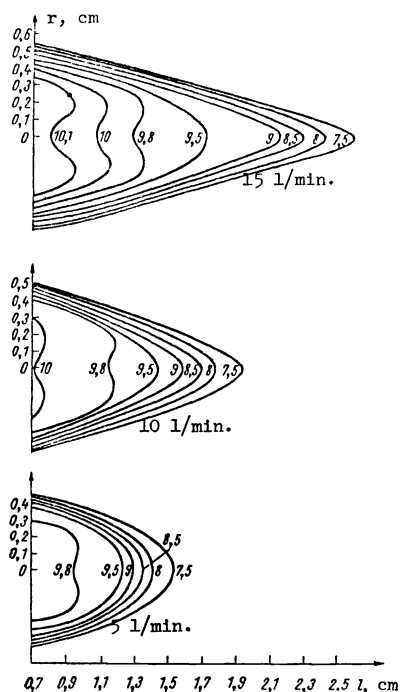and compiled by Dresvin, Ed. (ref. 24).

Fig. 12. Temperature map in the exit jet of
an inductin plasma at different total
plasma gas flow rates (gas: argon,
diam.: 14mm, f=17 MHz, P=6-8 kW)
(after Dresvin, Ed. (ref. 24.)

While most of the temperature measurements reported were made using argon as the plasma
gas, a few measurements are available for oxygen, air and nitrogen. The results given in
Fig. 13, show that the temperature field can change drastically with the change in the
plasma gas. The effect is reflected by a change in the maximum temperature attained in
the discharge. (7000 K for a nitrogen discharge compared to 9000 K for oxygen and 10500 K
for argon). Changing the plasma gas can also result in strong change in the shape and
size of the discharge as indicated in Fig. 14, in which complete temperature maps for an
argon and an oxygen plasma are given in the same torch under essentially the same opera-
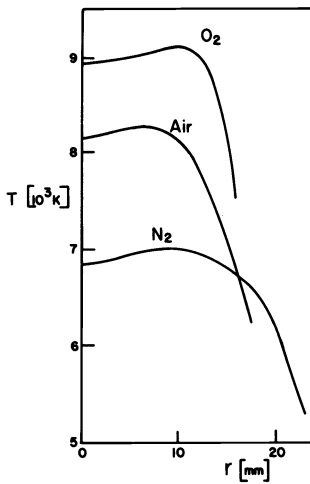ting conditions.

Fig. 13. Radial temperature profile at
  the mid-section of an induction plasma
  for different plasma gases
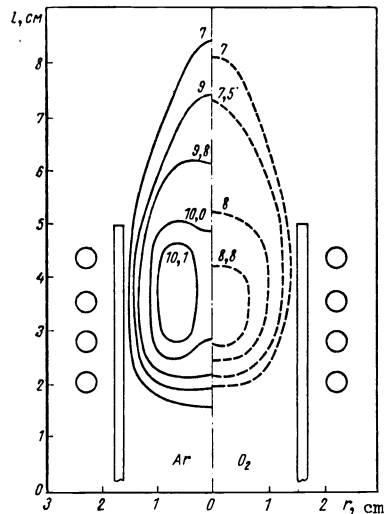 (after Dresvin, Ed. (ref. 25)).

Fig. 14. Temperature maps for argon
  and oxygen plasmas in the same plasma
  torch. In either case, Q_0=30 ℓ/min,
  and f=10 MHz. (a) Argon, P=12 kW
  (b) Oxygen plasma, P=8 kW
  (after ref. 26,27).

2.3-Velocity distribution

In contrast to the temperature measurements, velocity field measurements in inductively
coupled r.f. plasmas are rather complex and difficult to obtain. Most of the reported
measurements were carried out using water-cooled pitot or total impact tubes (ref. 18,
25-31). Tracer-photographic techniques have also been reported (ref. 28, 32-34) and most
recently laser-doppler-anemometry (LDA) (ref. 35-37).

While each of these techniques have their limitations they were mostly successful when ap-
plied to the measurement of the velocity profiles in the plasma jet at the exit of the
torch. The problem, however, is far more complex when it comes to measurements in the
coil region. So far, only the basic characteristics of the flow pattern in this region
were qualitatively observed.

One of the first investigations of the flow pattern in the coil region of the torch is
that due to Chase (ref. 28) who demonstrated the presence or recirculation motion in the
discharge using tracer techniques coupled with high speed photography.

Water-cooled pitot tube measurements were reported by Klubnikin (ref. 29) for a 40 mm
i.d. argon discharge excited at 6 MHz. The total power input was about 7.6 kW. The re-
sults shown in Fig. 15 show both the temperature map and a schematic of the flow pattern
in the discharge region for two gas flow rates. It is interesting to note the presence of
recirculation patterns in the coil region due to electromagnetic pumping. The position of
the recirculation vortex moves further downstream with the increase of the total plasma
gas flow rate. It may also be noted that at low gas flow rates there is an apparent en-
trainment of ambiant air in the torch.

Laser doppler anemometry measurements of the velocity profiles of the plasma jet at the
exit of an induction plasma torch were reported by Gouesbet et al. (ref. 35,36). These
were obtained for argon and argon/helium plasmas at atmospheric pressure at a power level
of 5 kW with a 30 mm i.d. plasma confinement tube. The argon gas flow rate was 21.1
ℓ/min. The results show that the addition of helium to the plasma gas, (0 - 0.7 ℓ/min)
had relatively little influence on the gas velocity which has a near parabolic profile
with a centerline maximum velocity of 15 m/s.

Gas and particle velocity measurements in the coil region of an induction plasma were re-
ported by Lesinski et al. (ref. 37) using laser doppler anemometry. A schematic of the
torch geometry and a summary of the operating conditions are given in Fig. 16. The plasma
gas was argon at atmospheric pressure. Measurements were reported of the velocity of the
plasma, and that of silicon partilces ($\bar{d}_p$= 33 μm & σ_s= 13 μm) introduced axially in the
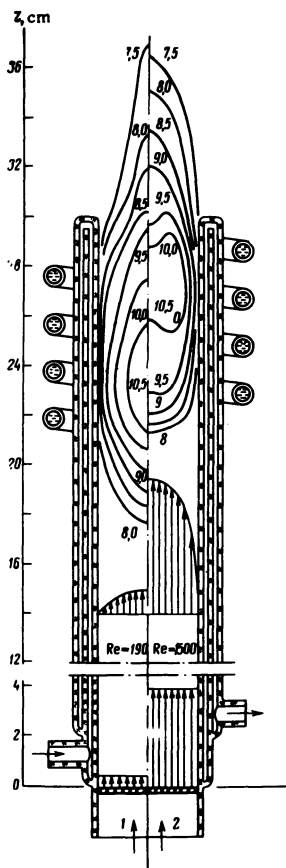plasma through a water-cooled powder feeding probe.

Fig. 15. Temperature map (left) and schematic of the flow pattern (right) for argon discharge at atmospheric pressure. 1. $Q_0=5$ ℓ/min; 2. $Q_0=40$ ℓ/min (after Klubnikin (ref. 29)).

DIMS. IN MM

f = 3MHz

n = 4 turns

$Q_2 = 11.7$ ℓ/min

$Q_3 = 63.0$ ℓ/min

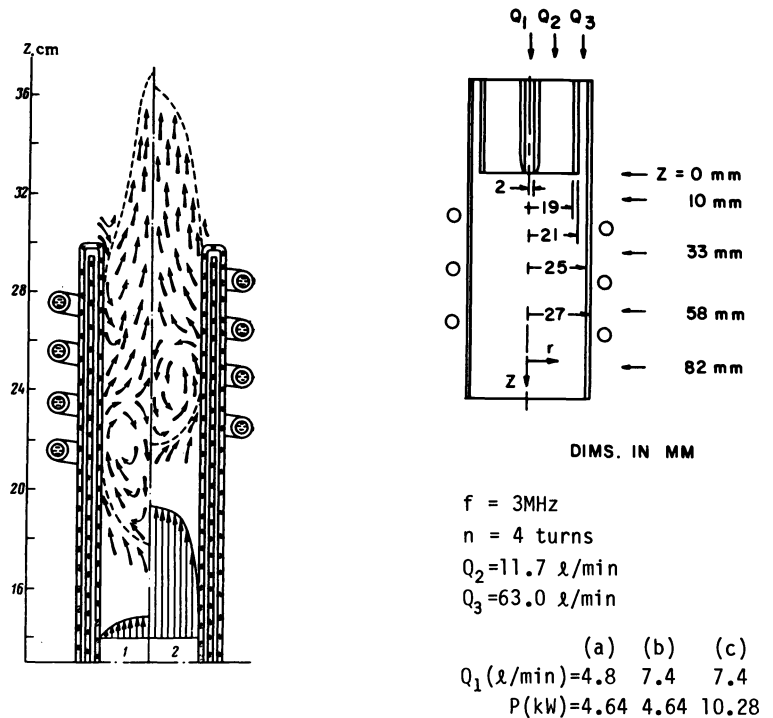|	(a)	(b)	(c)
Q_1(ℓ/min)=	4.8	7.4	7.4
P(kW)=	4.64	4.64	10.28

Fig. 16. Details of the induction torch geometry and operating conditions (after Lesinski et al. (ref.37)).

Typical results are given in Figs. 17 and 18 respectively. It is noted from Fig. 17, that, close to the point of injection ($0<z<35$ mm) the plasma velocity profiles are rather similar to that for a free jet. Further downstream they become increasingly flat with the mean velocity dropping rather slowly and reaches about 15-20 m/s at the exit of the torch. As expected, the centerline velocity in the torch increases with the increase in the powder carrier-gas flow rate, but much less so with the increase of the plasma power.

Similar velocity profiles were also obtained with the silicon particles under the same operating conditions, Fig. 18. It is noticed that in this case the particle velocity was systematically lower than that of the plasma. The difference is best demonstrated in Fig. 19, in which the axial velocity profiles of the plasma and the particles along the centerline of the torch are given. Included also, for comparison, are the axial velocity profiles for the gas in the torch at ambient conditions (i.e. without ignition of the plasma). In contrast to the plasma velocity profile, the cold gas axial velocity drops rapidly with distance along the axis of the torch.

2.4-Concentration distribution

Relatively little attention has been given to the gas mixing pattern in an induction torch. A study reported by Dundas (ref. 38) in 1970 gives measurements of the concentration field in a standard Model 66 TAFA torch. Measurements were made of the concentration profiles in the discharge region with argon as the plasma gas and either air or hydrogen as the sheath gas under different operating conditions. The plasma torch was operated using a power supply with an operating frequency in the range of 2.4-4.5 MHz. The net power in the discharge was approximately 13-16 kW. Typical results reported as concentration maps in the presence and absence of the discharge are given in Fig. 20.
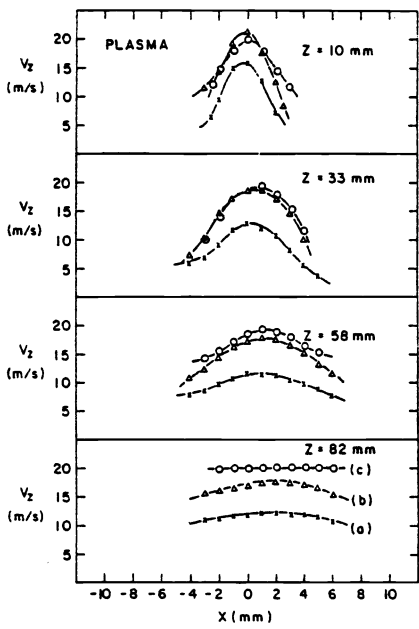
Fig. 17. Plasma velocity profiles over
the central region of the torch
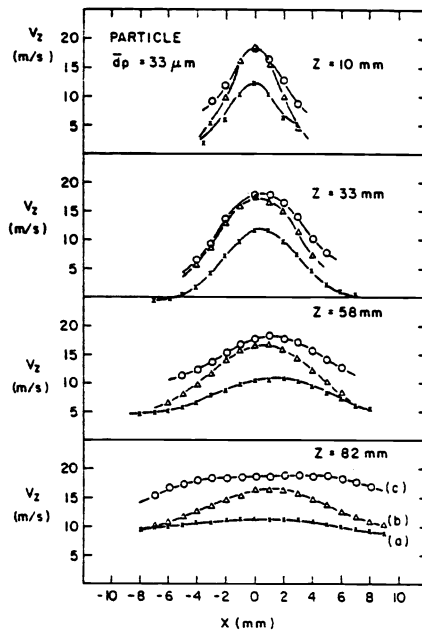(after Lesinski et al (ref. 37)).

Fig. 18. Particle velocity profiles
over the central region of the torch
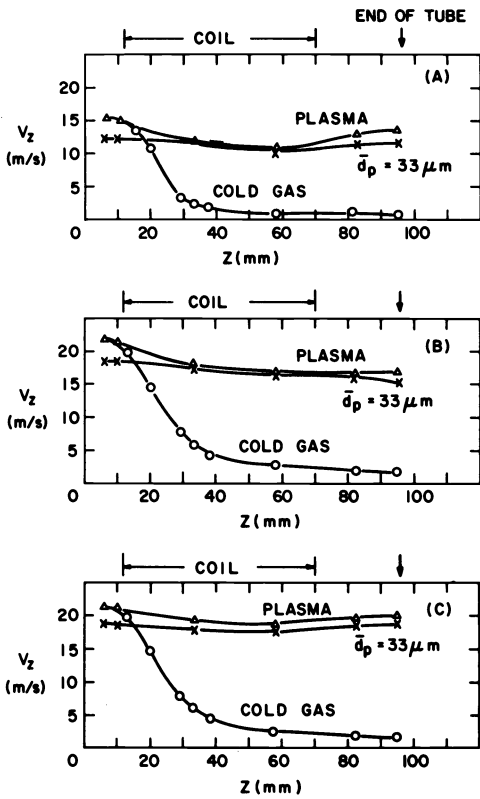(after Lesinski et al. (ref. 37)).

Fig. 19. Plasma and particle axial
velocity profiles along the centerline
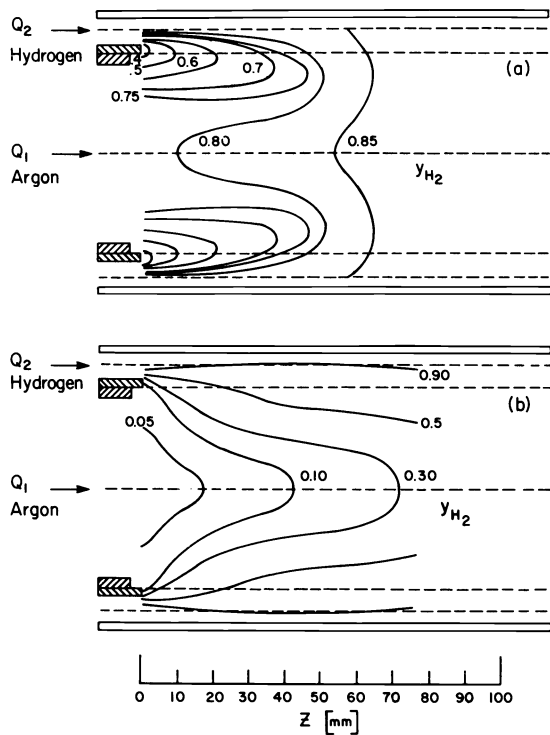of the torch
(after Lesinski et al (ref. 37)).

Fig. 20. Concentration maps for a
hydrogen/argon mass ratio of 1.67
(a) without the plasma, (b) with the plasma
(after Dundas (ref. 38)).

3-MATHEMATICAL MODELLING

Special attention has been given to the development of mathematical models for the quanti-
tative description of the phenomena which occur in the discharge region of an inductively
coupled plasma. These were mainly concerned with:

- Calculation of the temperature, flow and concentration distributions in the dis-
  charge

- Calculation of single particle or aerosol trajectories and temperature histories

- Plasma-particle interaction effects under dense loading conditions

In this section a brief review will be made of the principal models proposed underlining
their similarities and differences. Examples of typical results obtained under different
operating conditions are given.

3.1-Models of the temperature, flow and concentration fields

3.1.1-One-dimensional models. The first mathematical models proposed for the inductively
coupled plasma were one-dimensional (ref. 5,7,8,39-41). These were mainly concerned with
the calculation of the radial temperature profiles at the center of the discharge by an
energy balance between local energy generation and conduction and radiation heat losses.
In order to allow for the analytical solution of the governing equations, the models had
to be kept relatively simple and with few exceptions they adopted the following assump-
tions.

- Local thermodynamic equilibrium (LTE). As will be seen later this assumption has
  been maintained, for most of the one and two-dimensional models.

- Neglected convective heat transfer, with the exception of Keefer et al. (ref.
  41).

The proposed one-dimensional models differed, however, in the following.

- The degree to which they took into account the variation of the physical proper-
  ties of the plasma with temperature (Electrical and thermal conductivity).

- Whether or not they took into account in the energy equation radiation heat losses
  from the plasma.

Freeman and Chase (ref. 5) were the first to adopt the channel model described earlier in
section 1. Neglecting axial heat conduction, radiation and convective heat transfer, they
assumed that, under steady-state conditions, the energy dissipation in the core was balan-
ced by radial heat conduction to the wall of the plasma-confining tube. Solving the sim-
plified Elenbass-Heller equation and the Maxwell's equations, they calculated the power
density in the discharge for argon and nitrogen induction plasmas at atmospheric pressure
as a function of the magnetic field strength for operating frequencies between 250 kHz and
16 MHz.

In an attempt to refine the channel model Eckert (ref. 7) took into account the variation
of the electrical and thermal conductivity of the plasma across the core region. Assuming
a power-law distribution for the electric field and that the radius of the plasma column
was identical to that of the confining tube, Eckert obtained radial temperature profiles
in the discharge which were in general agreement with experimental data. Eckert (ref. 39)
later further modified this model and brought it "one step closer to reality" by including
the radiation losses in the analysis.

Mensing and Boedeker's (ref. 8) one-dimensional analysis of the inductively coupled plasma
was based on the simultaneous solution of the energy and the simplified Maxwell's equa-
tions taking into account both the conduction and radiation energy losses from the plasma.
Pridmore-Brown (ref. 40) solved the simplified energy, magnetic and electric fields equa-
tions as a two-point boundary value problem.

The only one-dimensional model to take convective heat transfer into account is that of
Keefer et al. (ref. 41). Their analysis was based on the numerical solution of the cor-
responding energy, electric and magnetic field equations. Only the radial convective term
was maintained and set to an arbitrary value. Their results showed the radial temperature
profile in the discharge region to be significantly influenced by the presence of an
inward radial gas stream.

Recently serious attempts were made by Eckert (ref. 42,43) and Aeschbach (ref. 44) to include non-equilibrium effects in a one-dimensional model for the ICP torch as used in spectrochemical analysis. Their results reveal important differences between the heavy particle and the electron temperatures in the immediate vicinity of the plasma confinement tube and in the center of the discharge in the presence of strong central flow.

3.1.2-Two-dimensional models. While the principal advantage of one-dimensional models is that they offer a relatively simple way of estimating the temperature profiles in the center of the discharge. They suffer from two main limitations. First, they provide no information about the temperature field outside the induction zone, and second, they can not be used for the calculation of the flow field in the torch. A number of two-dimensional models (ref. 45-54) were developed. These have the following points in common:

- They took into account conductive, convective and radiative heat transfer.

- The plasma was assumed to be optically thin.

- They all assumed local thermodynamic equilibrium (LTE).

- They took into account the variation of the thermodynamic and transport properties of the plasma with temperature.

- They maintained the one-dimensional electric and magnetic fields assumption.

They varied, however, in the following points:

- Whether, or not, they included the full momentum transfer equations.

- Whether they solved the transient or steady state equations. In either case they aimed at steady state solutions.

The first two-dimensional model of the inductively coupled plasma was that proposed by Miller and Ayen (ref. 45) who calculated the two dimensional temperature field by solving the corresponding energy equation simultaneously with the one-dimensional electric and magnetic field equations. They treated the radiation heat losses as a volumetric heat sink and assumed the plasma to be optically thin.

Since they did not take into account momentum transfer, they assumed the flow to be only in the axial direction and neglected radial convective transfer. At the inlet of the torch the velocity profile was taken as being flat with a step function increase of the velocity near the wall of the plasma confinement tube. As the plasma gas passed through the discharge zone, the axial velocity profile was allowed to change in such a way as to satisfy the principal of conservation of mass. The numerical technique used was based on the finite difference solution of the transient equations in discrete time steps until steady state conditions were reached.

Barnes and Schleicher (ref. 46) and Barnes and Nikdel (ref. 47,48) modified Miller's model to fit operating conditions used in spectrochemical analysis. They imposed on the flow a central jet stream to represent the aerosol carrier gas. Solving the continuity, energy, electric and magnetic field equations they calculated the flow and temperature fields under different operating conditions. Assuming similarity between the velocity and the concentration distribution of species in the torch they calculated spectral emittance distributions for elements from an injected sample and the continuum background radiation distribution.

While the above models represented an important step forward, it was obvious that a detailed understanding of the characteristics of the flow and temperature fields in the discharge region could only be achieved through the incorporation of the full momentum transfer equations. Independently Delettrez (ref. 49) and Boulos (ref. 50) calculated the two-dimensional velocity and temperature fields in the induction plasma by solving the corresponding continuity, momentum and energy equation simultaneously with the one-dimensional electric and magnetic field equations. Their mathematical approach was different, however, since Delettrez (ref. 49) solved the transient transport equations in terms of temperature and the axial and radial velocity components, while Boulos et al. (ref. 50-52), on the other hand, solved the steady state, two-dimensional momentum and energy equations in terms of the enthalpy, stream function and vorticity simultaneously with the one-dimensional electric and magnetic field equations and the phase difference between them.

The results obtained for an argon plasma at atmospheric pressure assuming laminar flow conditions, revealed an important influence of the electromagnetic forces on the flow field in the torch. This seems to be responsible for the formation of two recirculation eddies in the discharge region with the downstream eddy being swept-away with the increase of the plasma gas flow rate.

Recent work by Boulos and his collaborators (ref. 53,54) further refined this model and improved its computational stability by solving the continuity, momentum and energy equations in terms of their primitive variables, i.e. velocity, pressure and enthalpy rather than the stream function, vorticity and enthalpy used earlier. A different numerical algorithm is also used in this case. This is known as "Semi-implicit Method for Pressure-Linked Equations, Revised" or SIMPLER which was developed by Patankar and Spalding (ref. 55). A detailed comparison between the performance of the two computer codes is given by Mostaghimi et al. (ref. 53).

3.1.3-Governing equations and boundary conditions. For a typical induction plasma torch, Fig. 6, the two-dimensional continuity, momentum, energy and mass transfer equations can be written in terms of their primitive variables in the axially symmetric cylindrical system of coordinates as follow:

Continuity

$$\frac{1}{r} \frac{\partial}{\partial r} (r \rho v) + \frac{\partial}{\partial z} (\rho u) = 0 \tag{2}$$

Momentum transfer

$$\rho (v \frac{\partial u}{\partial r} + u \frac{\partial u}{\partial z}) = -\frac{\partial p}{\partial z} + 2 \frac{\partial}{\partial z} (\mu \frac{\partial u}{\partial z})$$

$$+ \frac{1}{r} \frac{\partial}{\partial r} \left[\mu r (\frac{\partial u}{\partial r} + \frac{\partial v}{\partial r}) \right] + \rho g \tag{3}$$

$$\rho (v \frac{\partial v}{\partial r} + u \frac{\partial v}{\partial z}) = -\frac{\partial p}{\partial r} + \frac{2}{r} \frac{\partial}{\partial r} (\mu r \frac{\partial v}{\partial r})$$

$$+ \frac{\partial}{\partial z} \left[\mu (\frac{\partial v}{\partial z}) + \frac{\partial u}{\partial r} \right] - \frac{2 \mu v}{r^2} - \xi \sigma E_\theta H_z \cos \chi \tag{4}$$

Energy transfer

$$\rho (v \frac{\partial h}{\partial r} + u \frac{\partial h}{\partial z}) = \frac{1}{r} \frac{\partial}{\partial r} (r \frac{k}{c_p} \frac{\partial h}{\partial r})$$

$$+ \frac{\partial}{\partial z} (\frac{k}{c_p} \frac{\partial h}{\partial z}) + \sigma E_\theta^2 - P_r \tag{5}$$

Mass transfer

$$\rho (v \frac{\partial y}{\partial r} + u \frac{\partial y}{\partial z}) = \frac{1}{r} \frac{\partial}{\partial r} (rD \frac{\partial y}{\partial r}) + \frac{\partial}{\partial z} (D \frac{\partial y}{\partial z}) \tag{6}$$

Where v and u are the plasma velocity components in the radial and axial directions respectively, h is the plasma specific enthalpy, y is the mass fraction of a given gaseous component in the mixture, r & z are distances in radial and axial directions, ρ, is the density, μ the dynamic viscosity, k the thermal conductivity, c_p the specific heat, D the diffusion coefficient, p is the local pressure and P_r, represents radiation losses per unit volume.

The corresponding one-dimensional electromagnetic field equations are:

$$\frac{1}{r} \frac{d}{dr} (rE_\theta) = - \zeta \omega H_z \sin \chi$$

$$\frac{dH_z}{dr} = - \sigma E_\theta \cos \chi \tag{7}$$

$$\frac{d\chi}{dr} = \frac{\sigma E_\theta}{H_z} \sin \chi - \frac{\zeta \omega H_z}{E_\theta} \cos \chi$$

Where E_θ is the electric field intensity in the θ direction, H_z, the axial magnetic field intensity and χ the phase difference between them; ω is the oscillator angular frequency ($\omega = 2\pi f$), σ the electrical conductivity of the plasma and ξ the magnetic permeability of free space.
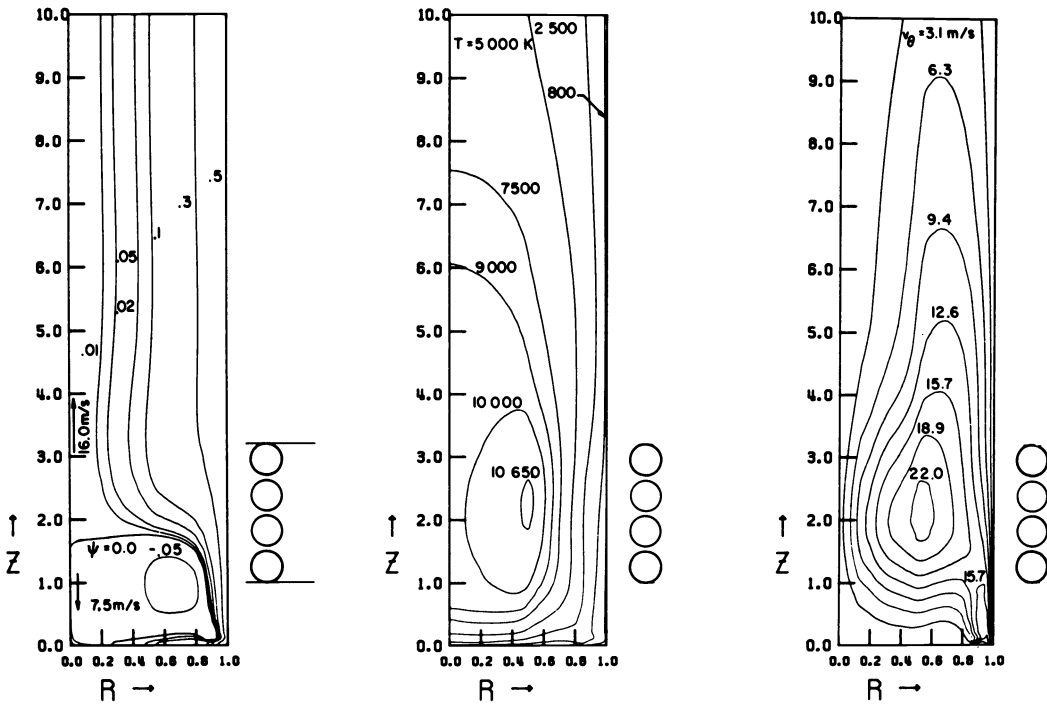
Fig. 21. Flow and temperature fields for a confined plasma in the presence of swirl, f=3 MHz, P_t=3.0 kW, Q_1=0.0, Q_2=2.0, Q_3=18.0 ℓ/min and $\bar{v}_\theta$=13.3 m/s (after Boulos et al. (ref. 51)).
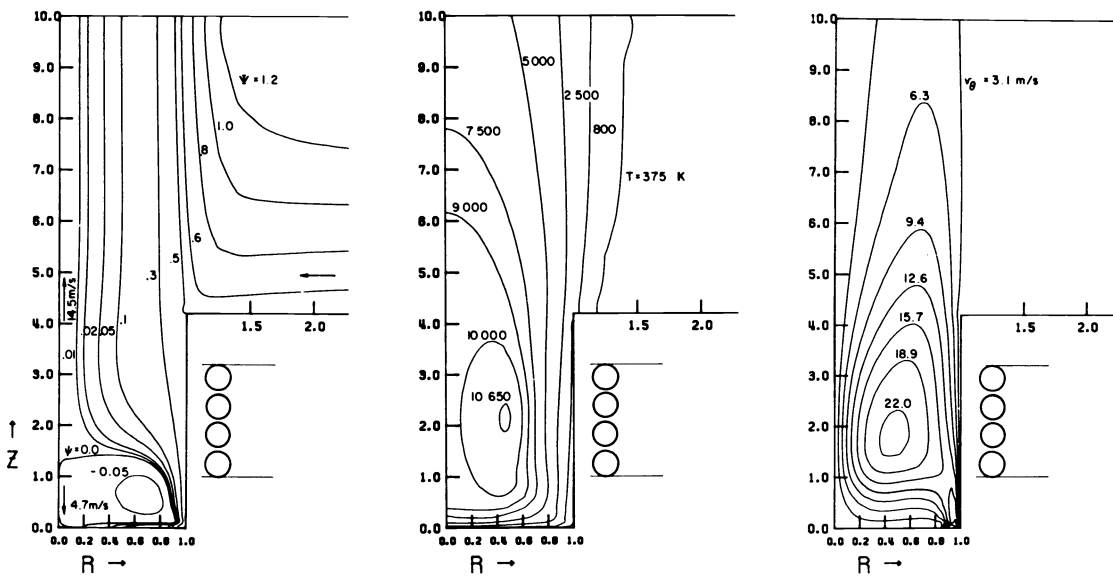

Fig. 22. Flow and temperature fields for a plasma under free discharge conditions in the presence of swirl f=3 MHz, P_t=3.0 kW, Q_1=0.0, Q_2=2.0, Q_3=18.0 ℓ/min and v_θ=13.3 m/s (after Boulos et al. (ref. 51)).

It is also observed that at Q_1=1.0 (ℓ/min) there is a strong circulation in the coil region and a small secondary recirculation zone near the wall (Fig. 23-a). As the central injection is increased, the circulation eddy becomes weaker and the back flow on the centerline eventually disappears. By contrast the recirculation zone on the wall becomes systematically larger.

Figure 24 shows the effect of the central injection on the velocity profile along the centerline. For Q_1 (ℓ/min) the backflow has a maximum velocity of about 7.0 (m/s) while the maximum velocity downstream of the coil is about 13 (m/s). With the increase of the central flow to 3.0 (ℓ/min), the backflow completely disappears and for Q_1=7.0 (ℓ/min) the central jet goes right through the coil region before it starts to decay.

Figure 25 shows the corresponding effect of the central jet on the temperature profile along the centerline of the torch. As expected there is a systematic drop in the maximum temperature and for Q_1=7.0 (ℓ/min) the gas maintains its inlet temperature for the full length of the coil region.

The radial temperature profiles in the middle of the coil, given in Fig. 26, show that increasing the central injection flow rate results in substantial lowering of the temperature along the axis accompanied by a slight increase in the temperature close to the wall of the plasma confinement tube.

Similar computations were also carried out for a nitrogen plasma at atmospheric pressure. The results showed that in spite of the fact that the power level was considerably higher for the nitrogen plasma (10 kW) compared to that for the argon plasma (3 kW), the temperature of the plasma was lower, showing a maximum value slightly above 7500 K. The velocities in the nitrogen plasma, on the other hand, were close to 1.5 times higher than those for the argon discharge.

3.1.4-Typical results. As an illustration of the present induction plasma modelling capabilities, typical results in terms of the calculated flow, temperature and concentration fields obtained using the above model with the appropriate boundary conditions will be given in this section. The computations were mostly carried out for atmospheric pressure argon and nitrogen plasmas. The range of torch dimensions and operating conditions used is summerized in Table 2.

<p align="center">Table 2: Torch sizes and operating conditions</p>

Tube Diameter	d_0=18 - 50 mm
Frequency	f = 0.3 - 26.3 MHz
Power in the plasma	P_t=1 - 15 kW
Total gas flow rate	Q_0=10 - 50 ℓ/min
Powder or aerosol carrier gas flow rate	Q_1=0.0 - 7.0 ℓ/min
Inlet swirl velocity	v_θ=0 - 20 m/s

It may be noted that one of the obvious applications of the present models was to determine the effect of the different operating parameters on the flow and temperature field in the discharge.

i) Effect of confinement. In order to determine the effect of plasma confinement, computations were made for a confined and a free plasma discharge under the same operating conditions. In the free plasma discharge case the plasma confining tube, while having the same diameter as that used for the confined plasma calculations, extendes only 15 mm beyond the end of the induction coil. At this point the plasma emerged as a free jet in an ambiant atmosphere which was assumed to be the same as the plasma gas (argon). In both confined and free plasma cases, the dimensions of the induction coil and the gas distributer were identical.

Typical streamlines, temperature and swirl contours obtained for a plasma oriented vertically upwards under free discharge conditions and with an inlet average swirl velocity of 13.3 m/s are given in Figs. 21&22. It is noticed that the flow field in the induction zone is similar to that obtained for the confined plasma under the same operating conditions. Beyond the confinement region, the hot plasma gas streams vertically upwards entraining a substantial amount of ambient gas. As shown in Fig. 22-a, the mass flow rate of the entrained gas, as indicated by the values of the stream function, ϕ, can be larger than the plasma gas itself. The entrained gas, however, does not seem to mix with the plasma tail flame and hardly exerts an influence on the centerline axial velocity.

It is noticed from Fig. 22-b that there is little change in the temperature field in the
coil region under confined or free discharge conditions. As the gases emerge from the
confining tube, however, they heat-up the ambient gas giving rise to its typical laminar
flame contours. It should be pointed out that calculations made with different plasma gas
flow rates showed an increase in the expansion of the discharge at the exit of the torch
with decreasing plasma gas flow rate.

As to the tangential velocity field, it can be noted from Fig. 22-c that in spite of the
relatively high swirl velocity in the sheath gas at the inlet of the torch (19.8 m/s) the
tangential velocity field decays to less than 7 m/s at the exit of the plasma confinement
tube.

ii) Effect of the central carrier gas. The effect of central injection on the flow and
temperature fields for a confined plasma are also investigated (ref. 54). The torch geo-
metry in this case was similar to that illustrated on Fig. 6 with R_0=25 mm, R_C=33 mm,
r_1=1.7 mm, r_2=3.7 mm, r_3=18.8 mm, L_1=10 mm, L_2=74 mm, L_T=250 mm and w=2.0 mm. Computa-
tions were carried out with the momentum and energy equations written in terms of their
primitive variables for both argon and nitrogen plasma gas.

Figure 23 shows the calculated isotherms and stream lines for an argon plasma with an
oscillator frequency of 3 MHz, a power level of 3 kW, and different central injection flow
rates (Q_1=1.0-7.0 ℓ/min). It is to be noted that the corresponding plasma gas flow rate,
Q_2, is kept constant while the sheath gas flow rate, Q_3, is adjusted in such a way so that
the total flow rate, Q_0, is constant. As the central injection flow is increased, the
entrance region close to the centerline cools down and the high temperature region (T>9600
K) is pushed closer to the wall of the plasma confinement tube. The temperature and flow
fields at the exit of the torch do not change appreciably with the increase of Q_1 over the
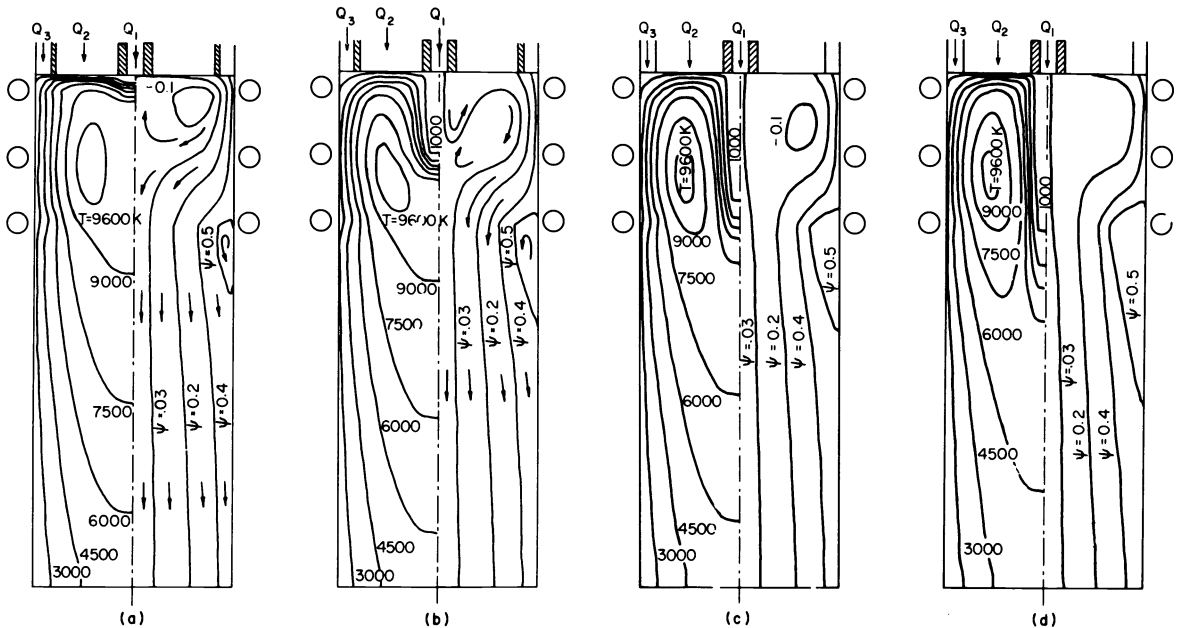range investigated.

Fig. 23. Isotherms (left) and streamlines (right) for argon plasma, P_0=3 kW, Q_0=20 ℓ/min
(a) Q_1=1 ℓ/min (b) Q_1=3 ℓ/min (c) Q_1=5 ℓ/min (d) Q_1=7 ℓ/min (after Mostaghimi et al.ref. 54)

iii) Effect of the total gas flow rate. Computations were carried out to determine the
effect of increasing the total gas flow rate, Q_0, on the flow and temperature fields in
the torch. In this case, Q_1 is kept zero while Q_2 and Q_3 are proportionnally increased to
give values of Q_0 varying between 20 and 50 (ℓ/min). The plasma gas is taken as argon
at atmospheric pressure and the total power level is 5 kW. The results indicate that
increasing the sheath gas flow rate considerably cools down the regions close to the wall
of the plasma confinement tube. Since the comparison is carried out for a constant total
power dissipated in the plasma, a corresponding increase of the temperature in the current
carrying region is observed.

For a total flow rate of 20 (ℓ/min), the local heat loss through the wall reaches its ma-
ximum value close to the downstream end of the coil (Fig. 27). This seems to coincide
with the stagnation point where the secondary recirculation zone on the wall starts. As
the flow rate is increased, a considerable reduction in the heat flux to the wall, in the
coil region, is observed. The point of maximum heat flux, however, moves systematically
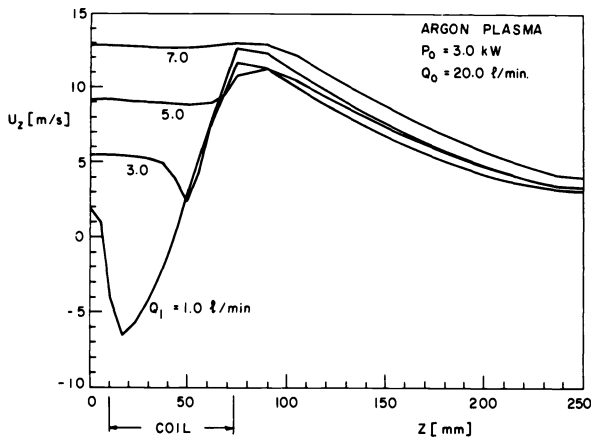downstream of the induction coil.

Fig. 24. Velocity profile along the centerline for an argon plasma (see Table 3-2 for the operating conditions). (after Mostaghimi et al. (ref. 54)).
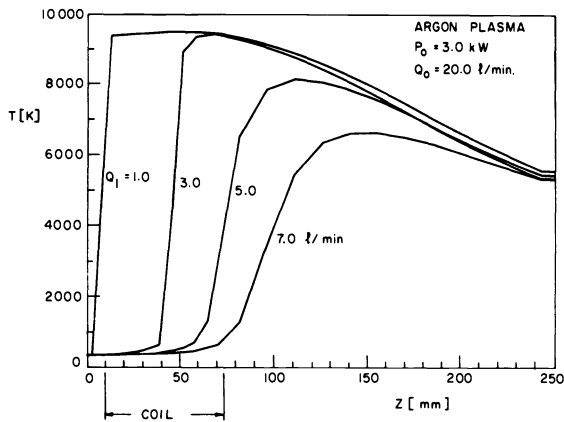

Fig. 25. Temperature profile along the centerline for an argon plasma (see Table 3-a for the operating conditions) (after Mostaghimi et al. (ref. 54)).

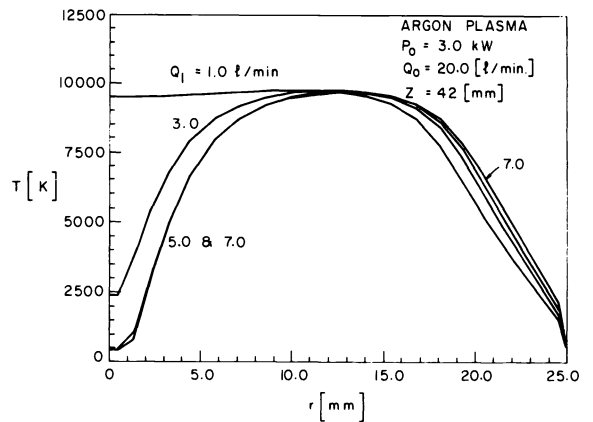Fig. 26. Temperature profile in the middle of the coil region for an argon plasma (see Table 3-a for the operating conditions) (After Mostaghimi et al (ref. 54)).
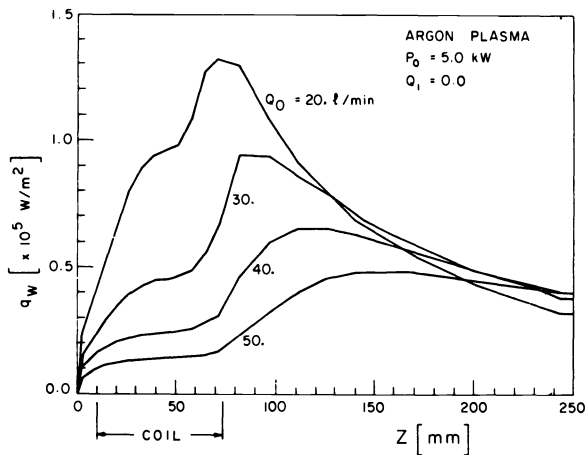

Fig. 27. Effect of the total gas flow rate, $Q_0=$, on the conduction losses to the wall (after Mostaghimi et al (ref. 54)).
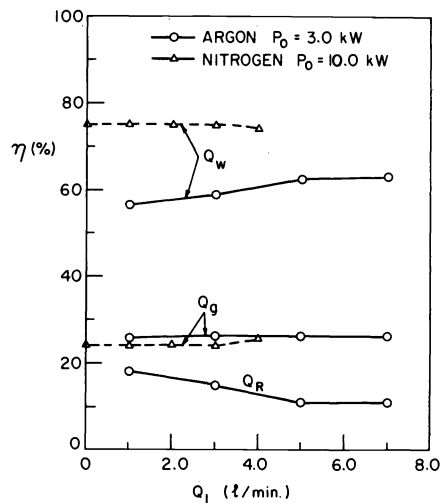

Fig. 28. Distribution of power for an argon plasma as a function of the total flow rate (after mostaghimi et al (ref. 54)).

Figure 28 shows the overall energy balance for that particular torch geometry and dimensions. It is noted that the radiation losses are virtually unchanged, whereas the heat loss by conduction to the wall decreases, and the enthalpy of the gas at the exit of the torch increases, almost linearly with the increase of the total gas flow rate. The specific enthalpy of the exit gas, on the other hand, does not seem to change substantially.

3.2-Single particle trajectories and temperature histories

Since the thermal treatment of powders in plasma torches and furnaces represents one of the most important applications of plasma technology, it is not surprising that considerable attention has been given to the important problem of plasma-particle heat transfer. A number of mathematical models have been developed for the thermal treatment of powders in d.c. plasma torches (ref. 57-62) and a few were applied to the induction plasma (ref. 63-68). In either case, the models differed in the assumptions made and whether or not they took into account the effects of internal heat conduction in particles on the overall heat transfer process between the plasma and the particles. Only Fiszdon (ref. 60) and Yoshida and Akashi (ref. 64) followed the internal heat conduction in the particles while the others assumed the particles to have a uniform temperature.

The specific question of whether, and when, is it necessary to take into account the internal heat conduction in the particles has been studied by Bourdin et al (ref. 69) and Chen and Pfender (ref. 70). The results reported by Bourdin et al (ref. 69) showed that differences as high as 1 000 K could develop between the surface temperature and that of the center of alumina particles as small as 20 μm in diameter when immersed in a nitrogen plasma at 10 000 K. The controlling parameter seems to be the Biot number which is simply the ratio of the thermal conductivity of the plasma to that of the particle (k/k_s). According to Bourdin et al. (ref. 69), during the transient heating of a particle under plasma conditions, internal heat conduction in the particle should be taken into account if the Biot number is greater than 0.02. The work of Chen and Pfender (ref. 70) on the other hand indicate that inspite of the differences in initial heating, the analytical expression based on infinite thermal conductivity predict the correct total time for both heating and evaporation even for low- conductivity materials such as alumina.

Chen and Pfender (ref. 71-73) also studied the evaporation of single particles under plasma conditions and the behaviour of small particles in a thermal plasma flow. In the latter case they propose a Knudsen number correction of the heat transfer rate to the particles to account for deviations from continuum fluid mechanics which becomes increasingly important for submicron particles.

In this section an outline will be given of the models proposed for the calculation of the trajectory and temperature history of single particles as they are injected in the discharge region of an inductively coupled plasma. The discussion will be limited to dilute systems which implies that the particle loading is sufficiently low so as to have neither an influence on the plasma flow and temperature fields, nor any particle-particle interaction effects.

For simplicity, the additional assumption of uniform particle temperature will be maintained throughout. The important problem of plasma-particle interaction will be discussed separately in section 3.3.

3.2.1-Governing equations.

Assuming that the only forces affecting an individual particle trajectory, are the drag and the gravity, the momentum equations for a single particle injected vertically downward into the plasma can be expressed as (ref. 63);

$$\frac{du_p}{dt} = -\frac{3}{4} C_D (u_p - u) |U_R| \left[\frac{\rho}{\rho_s d_p}\right] + g \tag{8}$$

$$\frac{dv_p}{dt} = -\frac{3}{4} C_D (v_p - v) |U_R| \left[\frac{\rho}{\rho_s d_p}\right] \tag{9}$$

with:
$$U_R = \sqrt{(u_p - u)^2 + (v_p - v)^2} \tag{10}$$

Where u_p and v_p are the axial and the radial particle velocities respectively, U_R is the relative speed between the particle and the plasma gas, d_p is the particle diameter and C_D is the drag coefficient which can be estimated as function of the particle Reynolds number ($Re = \rho U_R d_p / \mu$) using the following relations (ref. 63).

$$C_D = \begin{cases} \frac{24}{Re} & Re < 0.2 \\ \frac{24}{Re} (1 + \frac{3}{16} Re) & 0.2 < Re < 2.0 \\ \frac{24}{Re} (1 + 0.11 Re^{.81}) & 2.0 < Re < 21.0 \\ \frac{24}{Re} (1 + 0.189 Re^{0.62}) & 21.0 < Re < 200 \end{cases} \tag{11}$$

The particle temperature is determined by an energy balance between conductive and convective heat transfer between the particle and the plasma and radiative energy loss from the particle to the surrounding. The energy transfer equation can be written for a single particle as follows:

$$Q = \pi \, d_p^2 \, h_c \, (T - T_p) - \pi \, d_p^2 \, \sigma_{sb} \epsilon \, (T_p^4 - T_a^4) \tag{12}$$

Where Q is the net heat exchange between the particles and its surroundings,

$$Q = \begin{cases} (\frac{\pi}{6} \, \rho_p \, d_p^3 \, c_{ps}) \, \frac{dT_p}{dt} & \text{for } T < T_m \text{ and } T_m < T < T_v \\ (\frac{\pi}{6} \, \rho_p \, d_p^3 \, H_m) \, \frac{dx}{dt} & \text{for } T = T_m \\ - (\frac{\pi}{2} \, \rho_p \, d_p^2 \, H_v) \, \frac{dd_p}{dt} & \text{for } T = T_v \end{cases} \tag{13}$$

and

$$Nu = (\frac{h_c d_p}{k}) = 2.0 + 0.515 \, Re^{0.5} \tag{14}$$

h_c is the heat transfer coefficient, σ_{sb} is the Stefan-Boltzman constant, ϵ isthe particle emissivity, c_{ps} is the specific heat of the solid or liquid, particles, x is the liquid mass fraction of the particle, and T_p, T_m, T_v are the particle temperature, melting temperature, and the boiling temperature, respectively. H_m and H_v are the corresponding latent heat of melting and evaporation, respectively.

3.2.2-Typical results. As an example, the trajectories of fine alumina particles with a diameter of 10-200 μm injected in the discharge region of a confined argon induction plasma are given in Fig. 29 (ref. 63). A summary of the pertinent physical properties of pure alumina used in these calculations is given in Table 3. In this case, the plasma confinement tube had an internal diameter of 28 mm. The central powder carrier gas, intermediate and sheath gas flow rates were set to 0.4, 2.0 and 16.0 ℓ/min, respectively. The oscillator frequency was 3 MHz and the net power dissipated in the discharge was 3.77 kW.

In the representation of the trajectories given in Fig. 29, the size of the circles used to indicate the position of the particles is also an indication, although not to scale, of their diameter. Moreover, an open circule indicates a solid particle while a dark circle represents a liquid droplet.

It is obvious that the predictions which could be made using such a model can be very useful when it comes to the optimization of the injectin condition of a given powder or an aerosol with the objectives of obtaining either a physical and/or chemical change in the powder or simply evaporating them completely as it is the case in spectrochemical analysis.

Table 3: Summary of the physical properties of pure alumina (ref. 63)

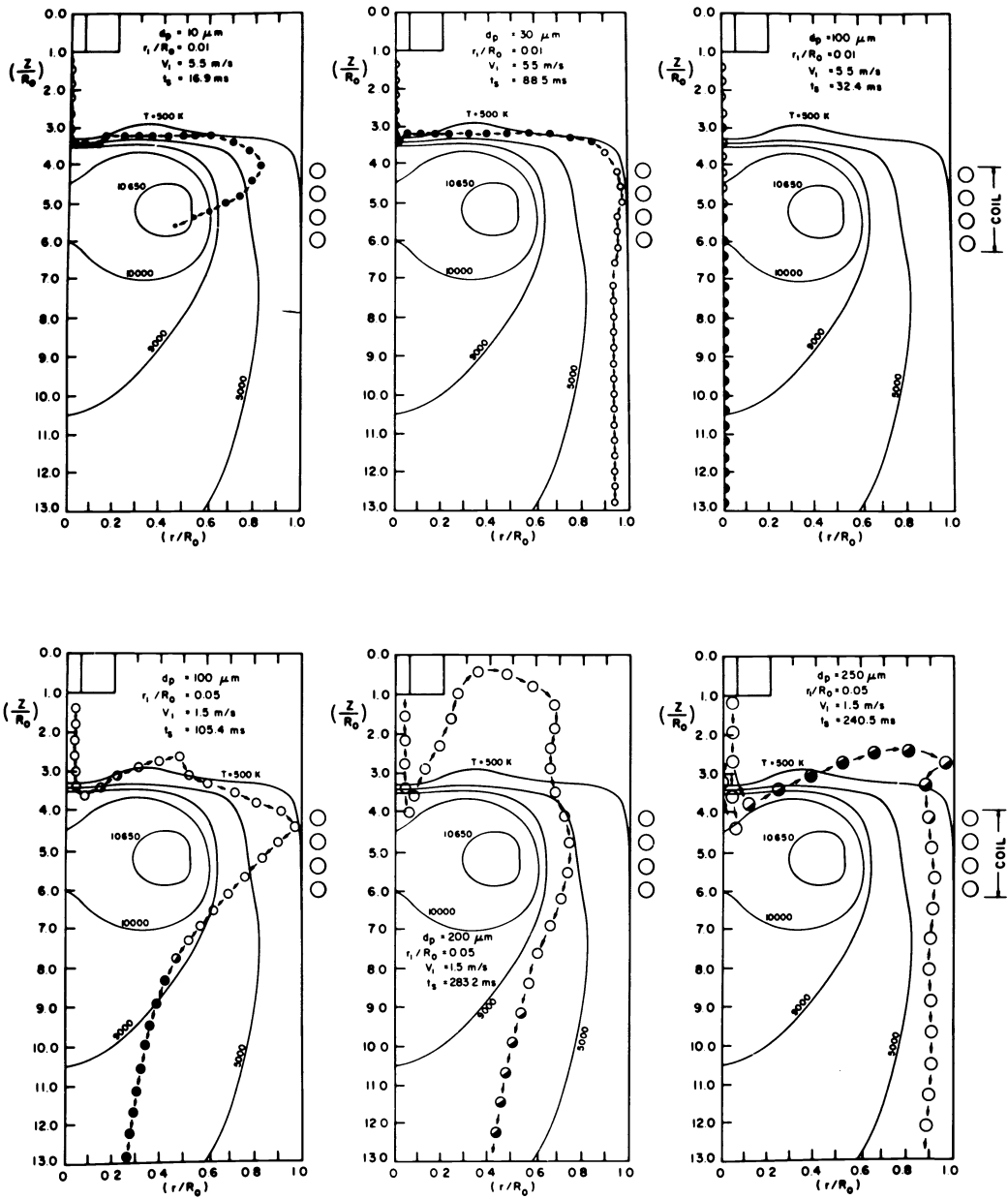|	
Density	ρ_s = 3900 kg/m³
Melting point	T_m = 2323 K
Laten heat of fusion	H_m = 1071 kJ/kg
Boiling point	T_v = 3800 K
Laten heat of evaporatin	H_v = 24660 kJ/kg
Emissivity	ϵ = 0.3
Specific heat	c_{ps} = 1.038 kJ/kg K, at 500 K
	= 1.200 kJ/kg K, at 1000 K
	= 1.405 kJ/kg K, at 1510 K
	= 1.958 kJ/kg K, at 2575 K

Fig. 29. Particle trajectories for alumina powder injected in an induction plasma
f=3 MHz, P_t=3.77 kW, Q_1=0.4, Q_2=2.0, Q_3=16.0 ℓ/min, v_θ=0
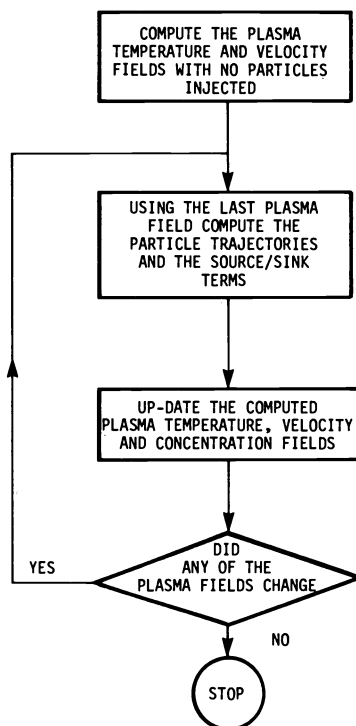(after Boulos (ref. 63)).

Fig. 30. Flow chart of the computatyional method
    (after Proulx et al. (ref. 68)).

3.3-Plasma-particle interaction effects

While the assumption of dilute system has generally been accepted for the calculation of individual particle treajectories and temperature histories under plasma conditions, the interpretation of the results obtained is greatly hindered by the simple fact that any application of plasma technology for the in-flight processing of powders will have to be carried out under sufficiently high loading conditions in order to make efficient use of the thermal energy available in the plasma. With the local cooling of the plasma due to the presence of the particles, model predictions using the low-loading assumption can be substantially in error.

In an attempt to take into account the plasma-particle interaction effects, Boulos and his collaborators (ref. 68) developed a mathematical model which through the iterative procedure illustrated in Fig. 30 up-dates continuously the computed plasma temperature, velocity and concentration fields. The interaction between the stochastic single particle trajectory calculatins and those of the continuum flow, temperature and concentration fields is incorporated through the use of appropriate source-sink terms in the respective continuity, momentum, energy and mass transfer equations. These are estimated using the so-called particle-source-in-cell model (PSI-Cell) (ref. 74) which can be represented schematically as shown in Fig. 31.

3.3.1-Governing equations. According the PSI-Cell model, the passage of a particle through a finite difference cell (Fig. 31) would result in the exchange of momentum, energy and mass between the particle and the fluid in that cell. To account for such an exchange it is necessary to add to each of the Eqs. 2-6, appropriate source-sink terms defined as S_p^C, S_p^{Mz}, S_p^{Mr} and S_p^C, respectively.

The formulation of these source terms deserves special attention.

Let N_t^c be the total number of particles injected per unit time, n_d is the particle size distribution, and n_r represents the fraction of N_t injected at each point over the central tube radius (Fig. 31). The total number of particles per unit time travelling along

the trajectory (ℓ,k) corresponding to a particle diameter $d_{p\ell}$ injected at the point r_k is:

$$N^o(\ell,k) = n_{d\ell} \, n_{rk} \, N_t^o \tag{15}$$

The particle concentration in a given cell crossed by the trajectory (ℓ,k) is;

$$C_{ij}(\ell,k) = \frac{N^o(\ell,k) \, \tau_{ij}(\ell,k)}{V_{ij}} \tag{16}$$

Where $\tau_{ij}(\ell,k)$ is the residence time of the (ℓ,k) particles in the (ij) Cell of volume V_{ij}. The mass source term for the (ij) Cell, due to all the trajectories with initial diameter $d_{p\ell}$ and initial injection point r_k is given as;

$$S_{p,ij}^c = \sum_{\ell,k} C_{ij}(\ell,k) \frac{\Delta m_p(\ell,k)}{\tau_{ij}(\ell,k)} \tag{17}$$

$\Delta m_p(\ell,k)$ is the amount of mass evaporated by a particle with (ℓ,k) trajectory in Cell (ij). The corresponding source term in the energy equation includes the heat given to the particles $Q_{p,ij}(\ell,k)$, as well as the superheat needed to bring the particle vapors into thermal equilibrium with the plasma gas $Q_{v,ij}(\ell,k)$.

$$S_{p,ij}^E = \sum_{\ell,k} C_{ij}(\ell,k) \left(Q_{p,ij}(\ell,k) + Q_{v,ij}(\ell,k) \right) \tag{18}$$

where

$$Q_{p,ij}(\ell,k) = \frac{1}{\tau_{ij}(\ell,k)} \int_0^{\tau_{ij}(\ell,k)} \pi d_p^2 \, h_c \, (T_{ij} - T_{p,ij}(\ell,k)) \, dt \tag{19}$$

and

$$Q_{v,ij}(\ell,k) = \frac{1}{\tau_{ij}(\ell,k)} \int_0^{\tau_{ij}(\ell,k)} \frac{\pi}{2} d_p^2 \, \rho_s \, (\frac{dd_p}{dt}) \, c_{p_v} \, (T_{ij} - T_{p,ij}(\ell,k)) \, dt \tag{20}$$

Where c_{pv} is the specific heat of the particle material in vapour form. The source-sink terms for the corresponding momentum transfer equations are:

$r_1 = 1.7 [mm]$
$r_2 = 3.7 [mm]$
$r_3 = 18.8 [mm]$
$R_0 = 25.0 [mm]$
$R_c = 33.0 [mm]$
$L_1 = 10.0 [mm]$
$L_2 = 74.0 [mm]$
$L_T = 250. [mm]$
$W = 2.0 [mm]$
$Q_1 = 3.0 [\ell/min]$
$Q_2 = 3.0 [\ell/min]$
$Q_3 = 14.0 [\ell/min]$
$P_0 = 3.0 [kW]$
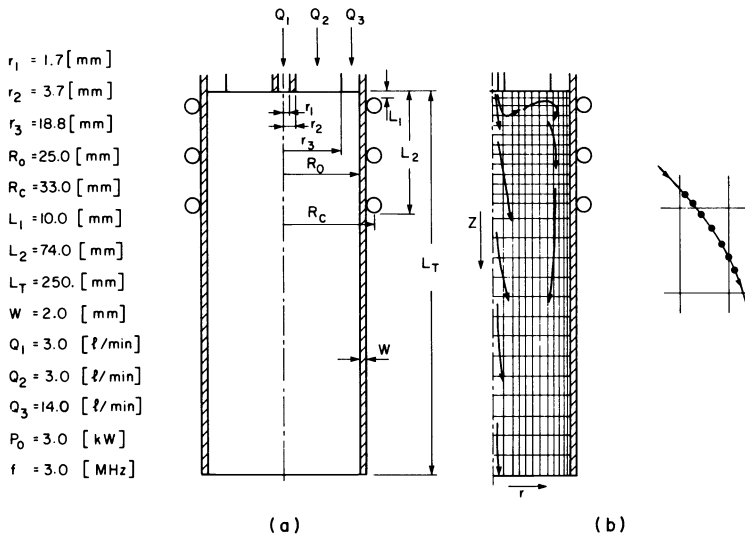$f = 3.0 [MHz]$

(a) (b)

Fig. 31. Schematics of the torch and the computational domain (after Proulx et al. (ref. 68)).

$$S^{Mr}_{p,ij} = \sum_{(\ell,k)} C^{(\ell,k)}_{ij} \frac{\Delta(m_p v_p)}{\tau^{(\ell,k)}_{ij}}$$ (21)

and

$$S^{Mz}_{p,ij} = \sum_{(\ell,k)} C^{(\ell,k)}_{ij} \frac{\Delta(m_p u_p)}{\tau^{(\ell,k)}_{ij}}$$ (22)

3.3.2-Typical results. As an example of possible plasma-particle interaction effects in induction plasma modelling under heavy loading conditions results reported by Proulx et al. (ref. 68) will be given in this section. These were obtained for an inductively coupled plasma torch operated with argon at atmospheric pressure. Details of the torch dimensions and operating conditions are given in Table (4-a).

Copper powder with a mean particle diameter of 70 μm and a standard deviation of 30 μm is injected through the central tube into the coil region of the discharge. The choice of copper made it possible to take into account the effect of the presence of copper vapour on the transport properties of the argon under plasma condition. For these, the data published by Mostaghimi and Pfender (ref. 75) were used which showed that the presence of even small amounts of copper vapour can have a pronounced effect on the electrical conductivity of argon.
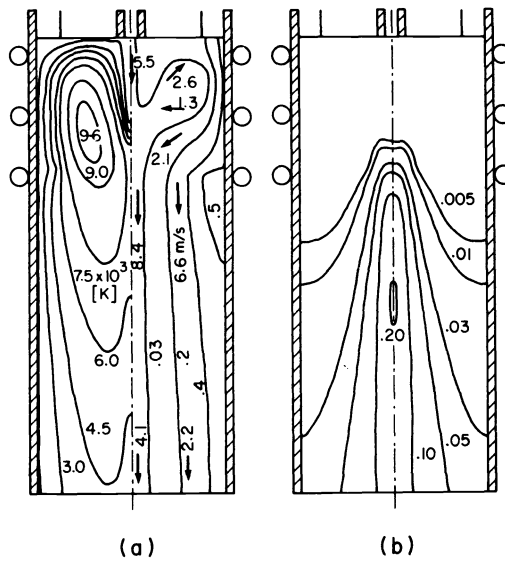

Fig. 32. (a) Isotherms and stream lines for 5.0 (g/min) copper feed rate
(b) Iso-concentration contours of copper vapor for this case
(after Proulx et al. (ref. 68)).

Dividing the Gaussian particle size distribution of the copper powder into, n_d, discrete fractions and their spatial distribution in the powder injection tube into, n_r, discrete positions, the problem simplifies to one of calculating $n_d \times n_r$ different possible trajectories. Assuming that the injection velocity of the particles to be equal to that of the carrier gas velocity at the point of injection, 35 such individual trajectories could be calculated corresponding to valves of n_d and n_r of 7 particle diameters and 5 injection points respectively. These were used to determine the effect of particle loading on the flow, temperature and concentration fields in the discharge.

Table 4-a: Torch dimension and summary of the operating conditions

r_1	= 1.7	(mm)	L_1	= 10.0	(mm)	Q_1	= 3.0	(ℓ/min)
r_2	= 3.7	(mm)	L_2	= 74.0	(mm)	Q_2	= 3.0	(ℓ/min)
r_3	=18.8	(mm)	L_T	=250.0	(mm)	Q_3	=14.0	(ℓ/min)
R_0	=25.0	(mm)	w	= 2.0	(mm)	P_0	= 3.0	(kW)
R_c	=33.0	(mm)				f	= 3.0	(MHz)

Table 4-b: Particle size distribution, feed rates and
overall energy exchange between the powder and the plasma

Material: Copper powder, $\bar{d}_p$= 70 μm, σ_s= 30 μm, ρ_s= 8900 kg/m³

T_m = 1356 K, H_m =204.7 kJ/kg, c_{ps}= 0.425 kJ/kg
T_v = 2840 K, H_v =4794.0 kJ/kg, c_{pv}= 0.480 kJ/kg

m_p (g/min)	m_v (g/min)	Q_p (w)	Q_v (w)	% of total energy absorbed
1.0	0.50	·71.0	21.0	3.1
5.0	1.40	255.0	42.0	9.9
10.0	1.40	386.0	35.0	14.0
15.0	1.16	460.0	28.0	16.3
20.0	0.94	511.0	23.0	17.8

Results were reported (ref. 68) for different mass feed rates of the copper powder varying between 1.0 and 20.0 g/min. Fig. 32 shows the isotherms, stream lines, and the concentration of copper vapor in the torch for a feed rate of 5 g/min. Because the trajectories of the particles in this case are very close to the axis of the torch, the plasma gas is significantly cooled down in this region (Fig. 33). On the other hand, the outer region of the plasma, where most of the power is dissipated, remains largely unaffected by the increase in the copper feed rate (Fig. 34). The result clearly demonstrates that although the overall loading ratio of the copper powder to plasma gas might be small (0.19 g copper/g argon), the local cooling effects are significant. This is a clear indication that the plasma-particle interactions effects could be locally very important under the loading conditions which are generally assumed to be safe to neglect the changes in plasma temperature due to the presence of the powder.

It should be noted that momentum transfer between the gas and the particles is found to be negligible, and that the flow field is affected only through the local plasma temperature changes. As the particles pass through the plasma, a portion of the powder evaporates and the vapor diffuses into the plasma medium (Fig. 32-b). The heat absorbed by the solid particles Q_p, and the superheat absorbed by the copper vapor to heat up to the plasma temperature Q_v, are given in Table 4.b. Q_v is generally much smaller than Q_p. The ratio Q_v/Q_p changes from 0.296 at 1.0 (g/min) feed rate to 0.045 at 20.0 (g/min) powder feed rate, and the total energy absorbed by the powder is between 3.1% and 17.8% of the plasma power input.

It should be pointed out that the plasma-particle interaction effect, through its influence on the flow and temperature fields in the discharge, could obviously have an important influence on the predicted particle processing efficiency. Figs. 41 and 42 gives typical particle temperature history profiles and average particle size, respectively in the presence and absence of loading effects.

It may be noted from Fig. 35 that the local cooling of the plasma due to the presence of the particles is responsible for the reduction of the heating rate of the particles as they are injected in the torch and the downstream shift of the point at which they reach their boiling point. The effect results in a corresponding reduction of mass fraction of the powder which is evaporated by the time the powder exits from the discharge. As shown in Fig. 36, for the copper powder with an initial mean particle diameter of 70 μm, the mean particle size at the exit of the torch is close to 60 μm for a powder feed rate of only 7.5 g/min, compared to a value of 40 μm for the no-loading case ($\dot{m} \approx 0$).
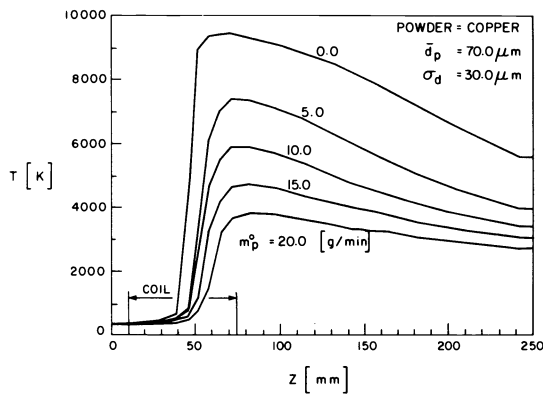
Fig. 33. Effect of particle feed rate on the temperature profile along the axis of the torch (after Prouls et al. (ref. 68)).
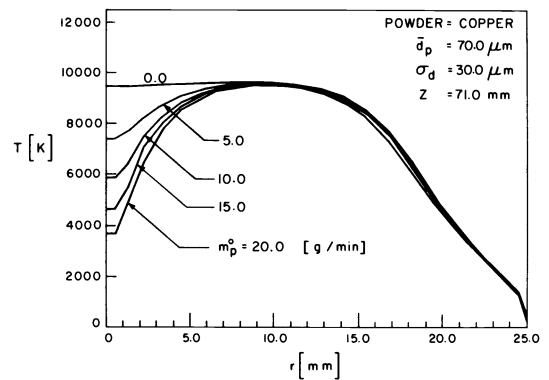

Fig. 34. Effect of particle feed rate on the radial temperature profile at z=71.0 mm (after Proulx et al. (ref. 68)).
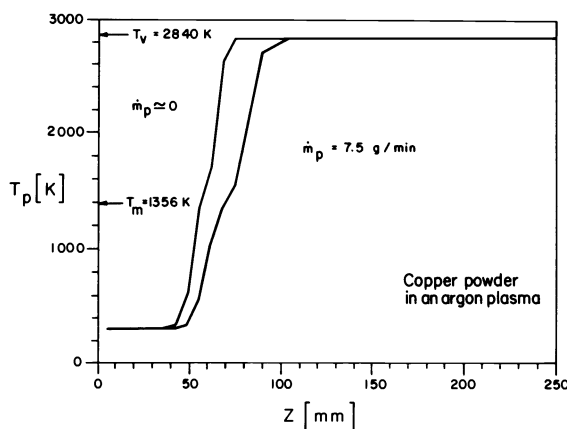

Fig. 35. Particle temperature history along the axis of the discharge in the presence and absence of particle-loading effects (after Proulx (ref. 65)).
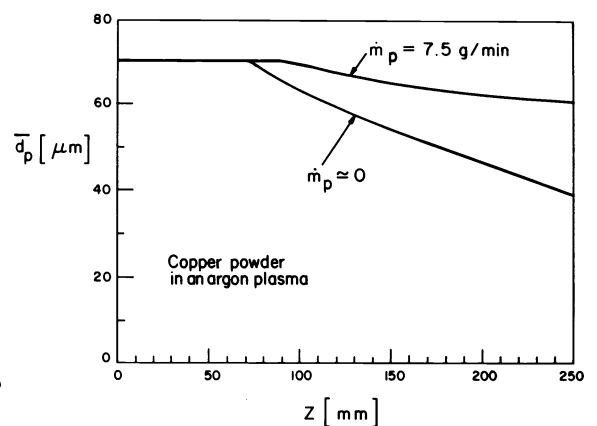

Fig. 36. Mean particle diameter along the axis of the discharge in the presence and absence of copper loading effects (after Proulx, (ref. 65)).

4-APPLICATIONS

While the inductively coupled plasma torch has long been considered as an excellent tool for fundamental laboratory plasma research, it has gradually found an increasing number of laboratory and industrial applications. In this section a brief review is made of the principal developments in this area. These are presented in three successive groups of applications; the first makes use of the plasma only as a heat source, the second involves chemical reactions, while the third involves spectrochemical effects.

4.1-Applicatons in which the plasma is used as a heat source

4.1.1-Crystal growth. Crystal growing is one of the first applications to be tested in the early sixties using the inductively coupled plasma (ref. 76-79). A schematic diagram of the apparatus used by Chase and Ruyven (ref. 78) is given in Fig. 37. The operation involved the injection of the powder in the center of the discharge and collecting the formed molten droplets on a target mounted in a muffle furnace on a suitable withdrawal mechanism. Among the materials tested are saphire, zirconia and niobium.

4.1.2-Sheroidization. A closely related application is the spheroidization of fine powders of metals, alloys or refractories. The technique is essentially similar to that used in crystal growth except that the molten droplets are allowed sufficient time for in-flight freezing as they immerge from the plasma before entering the collection system.

4.1.3-Plasma spray-coating and deposition. Recently, Jurewicz et al. (ref. 80) used the same concept of in-flight melting of powders in an induction plasma for the spray-coating and the deposition of structural pieces of metals and alloys under atmospheric pressure

and soft vacuum conditions.

Results obtained using, Ni, Ni-Cr, Cu, Ti and W, showed excellent quality of the deposits obtained with some deposits reaching an apparent density higher than 99.6% of the bulk material. Among the important advantages of this technique are:

●Ease of injection and long residence time of the powder in the plasma.
●Ease of melting of relatively large particles.
●The possibility of using substantially higher particle loading without loss of melting
 efficiency.
●Minimal sensitivity to operating conditions.
●Ability to obtain high density deposits.

Its principal disadvantage, however, lies in the physical difficulty of manipulating an induction torch to spray-coat a target of a relatively complicated configuration. In such a case it might be easire to manipulate the target rather than the torch.
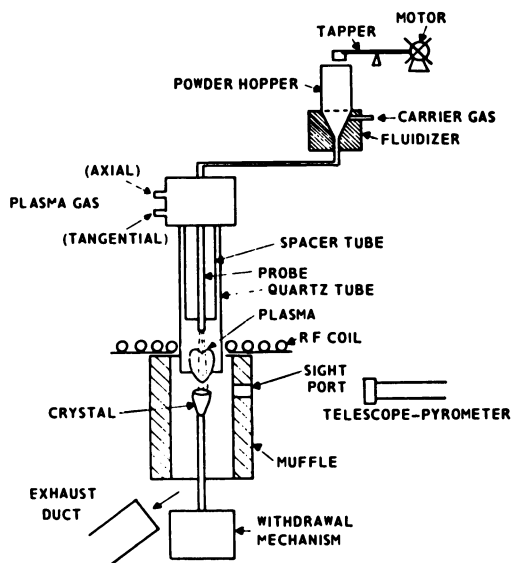

Fig. 37. Schematic of an experimental set up used for crystal growth
       (after Chase and Ruyven (ref. 78)).

4.1.4-Plasma sintering. Plasma sintering of ceramics represents also another interesting potential application of induction plasma technology in material processing. In this case the material to be sintered is passed axially through the plasma at velocities up to 1.0-3.0 cm/min. Results reported by Johnson and his collaborators (ref. 81-83) using alumina rods doped with MgO show considerable densification of the rod to well above 99%.

4.2-Applications involving a chemical reaction

4.2.1-Synthesis of high purity silicon. One of the important industrial applications of induction plasma technology is the synthesis of high purity fused silica with the low water content required for the fiber optic industry. In this particular case, the process takes full advantage of the principal characteristics of induction plasmas which is the high level of purity that can be maintained in the reaction chamber compared to other technologies.

A Schematic of the porcess developed by Naussau and Shiever of Bell Labs (ref. 84) is given in Fig. 38. The silica is produced in this case through the oxidation of $SiCl_4$ in an oxygen plasma; $SiCl_4 + O_2 \rightarrow SiO_2 + 2Cl_2$

The formed silica is collected in the shape of a boule on a SiO_2 pedestal. The shape of the formation depends on the boule temperature, and the position and size of the nozzle delivering the $SiCl_4$. Among the serious problems encountered are the formation of bubbles during the growth of the silica boule and the OH content of the produced silica which should be maintained in the low ppm if not in the ppb level.

4.2.2-Synthesis of pigment titanium dioxide. The synthesis of TiO_2 pigments modified by additives of Al_2O_3 through the oxidation of $TiCl_4$ vapour with an admixture of $AlCl_3$ in an oxygen plasma using induction plasma technology has been in commercial operation in the

USSR over the last ten years on a power level of 0.5-1.0 MW. The output of a 160 kW installation was reported (ref. 85) to reach as high as 5000 t per year with a specific power requirement of 1.93 kWh/kg of pigment.
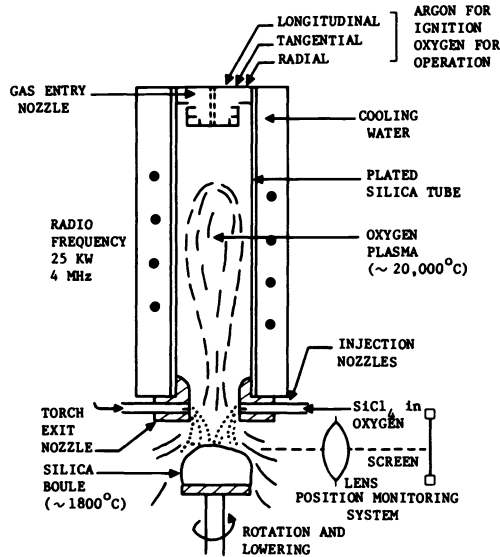
Fig. 38. Induction plasma torch arrangement for the production of fused SiO_2 (after Nassau and Shiever (ref. 84)).

4.2.3-Synthesis of ultrafine ultrapure powders. One of the potentially important applications of induction plasma technology is in the area of the synthesis of ultrafine ultra pure powders of metals and ceramic materials.

A significant effort has been devoted to this end by Akashi and his collaborators who worked on the synthesis of ultrafine iron particles (ref. 86), Titanium and silicon nitride (ref. 11,87), using the hydrid induction plasma torch.

The synthesis of ultrafine nitrides, oxides and carbides in an r.f. plasma has also been reported by Canteloup and Mocellin (ref. 88,89) and more recently by Hollabaugh et al (ref. 12) at the Los Alamos National Laboratory.

One common feature to the results obtained by the different investigators is the very small size of the powder obtained which are essentially an agglomerate of particles of the order of 10-20 nm in diameter. These gives rise to a high specific surface of the powder and offers considerable difficulty in their manipulation and further processing using standard powder metallurgy techniques. Obviously this is an area where further work is needed before we can achieve the required control on the particle size distribution of the product.

4.3-Spectrochemical elemental analysis
By far the use of the ICP as an emission source in spectrochemical analysis represents one of the widest applications of induction plasma technology, not in terms of the absolute power level, but rather in the number of commercially operated units around the world.

A schematic representation of the system used in this case is given in Fig. 39. As indicated, the solution to be analysied is injected as an aerosol in the discharge region of a relatively small, low power torch, 18 mm in diam. 1-2 kW, operated with argon as the plasma gas, and with either argon or nitrogen as the sheath gas. As the aerosol droplets crosses the discharge zone, they are evaporated, and the formed analyte granule evaporated and dissociated in turn. The intensity of emission for each of the elements in the analyte can be related, through a pre-calibration, to the original concentration of the analyte in the solution. Depending on the required dissociation, ionization and excitation energies, each element has its optimal observation hight for a set of operating conditions of

the plasma torch. The most commonly used observation zone is located between 15 and 20 mm above de coil.

Among the vast literature available, the review published by Barnes (ref. 90) and the books by Thompson and Walsh (ref. 91), Trassy and Mermet (ref. 92) and Bouman, Ed (ref. 93) gives an excellent overview of the subject.
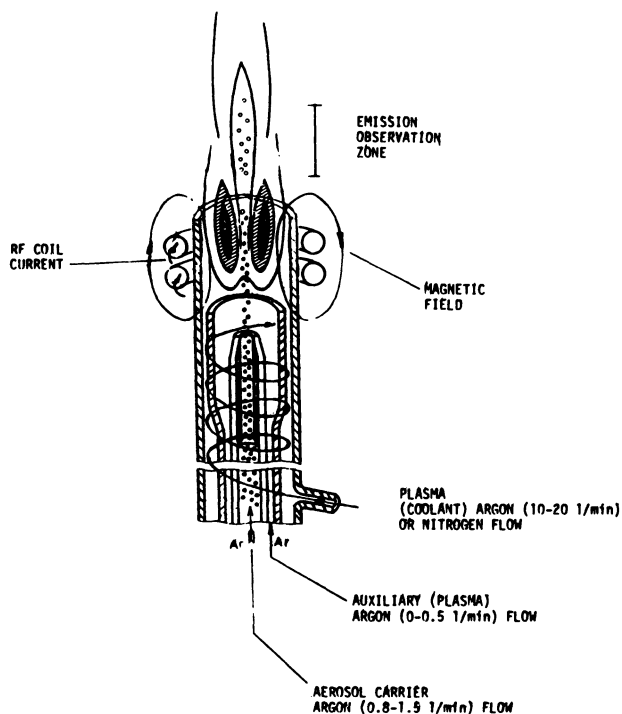

Fig. 39. A Schematic representation of the ICP discharge used in spectrochemical elemental analysis (after Barnes (ref. 90)).

REFERENCES

1. Babat, G.I., J. Inst. Elec. Eng., London, 94, 27 (1947).

2. Reed, T.B., J. Appl. Phys., 32, 821 (1961).

3. Eckert, H.U., High Temperature Science, 6, 99 (1974).

4. Davies, J. and P. Simpson, "Induction heating Handbook", McGraw Hill (1979).

5. Freeman, M.P. and Chase, J.D., J. of Appl. Physics, 39, 180 (1968).

6. Thorpe, M.L., and Scammon, L.W., "Induction plasma heating; high power, low frequency operation and pure hydrogen heating", TAFA final report under contract agreement #NSAU 3-9375 (1968).

7. Eckert, H.U., J. Appl. Phys., 41, 1520 (1970).

8. Mensing, A.E. and Boedeker, L.R., Theoretical investigations of R.F., induction heated plasmas", NASA CR-1312 (1969).

9. Vogel, C.E., Pool, J.W. and P. Dundas, "Radiation measurements and low frequency and high pressure investigations of inductin heated plasma", NASA CR-1804 (1971).

10. Pool, J.W., Freeman, M.P. Doak, K.W. and M.L. Thorpe, "Simulator tests to study hot-flow problems related to a gas core reactor". NASA CR-2309 (1973).

11. Yoshida, T., T. Tani, H. Nishimura and K. Akashi, J. Appl. Phys., 54, 640 (1983).

12. Hollabaugh, C.M., D.E. Hull, L.R. Newkirk and J.J. Petrovic, J. Mat. Sci, 18, 3190 (1983).

13. Eckert, H.U., J. Appl. Phys., 42, 3108 (1971).

14. Trekhov, E.S., Fomenko, A.F. and Khoshev, Yu, M., Teplofiz. Vys. Temp., 7, 860 (1969).

15. Eckert, H.U., J. Appl. Phys., 43, 2707 (1972).

16. Johnston, P.D., Brit. J. Appl. Phys., 1, 479 (1968).

17. Kleinmann, I. and Cajko, J., Spectrochim. Acta, 25B, 657 (1970).

18. Dresvin, S.V. and Klubnikin, V.S., Teplofiz. Vys. Temp., 9, 475 (1971).

19. Dymshits, B., Koretskiy, Ya. P., z. Tekhn Fiz., 34, 1677 (1964).

20. Goldfarb, V. and Dresvin, S.V., Toplofiz. Vys Temp., 3, 333 (1965).

21. Hughes, D.W., Wooding, E.R., Phys. Lett., A42, #1 (1967).

22. Vurgel', F.B. et al. Low Temperature Plasma, Edited by A. Ye Sheydlin, Moscow, Mir (1967).

23. Consoli, J., Proc. VI Intern. Conf. Ioniz. Phen. in Gases, Paris (1963).

24. Donskoi, A.V., Goldfarb, V.M. and Klubnikin, V.S., "Physics and Technology of low-temperature plasmas. S.V. Dresvin, Ed. (1972). English edition translated by T. Cheron and edited by H.U. Eckert. Iowa State University press (1977).

25. Goldfarb, V.M. et al., Teplofiz Vys. Temp., 5, #4 (1967).

26. Goldfarb, V.M. et al., Proc. XIV Coll. Sprectrosc. Intern. Debrecin, Hungary, p. 751 (1967).

27. Goykhman, V. Kh et al. Proc. I. Allunion Conf. Phys. Low-temp. plasma, Kiev, Nankova Dumka, p. 33 (1966).

28. Chase, J.D. J. Appl. Phys., 42, 4870 (1971).

29. Klubnikin, V.S., Teplofiz Vys. Temp., 13, 473 (1975). High Temp., 13, 439 (1975).

30. Dresvin, S.V., and Kh. El'-Mikati, Teplofiz Vys. Temp., 15, 1158 (1977).

31. Waldie, B. and R. Hancock, Trans. I. Chem. Eng., 56, 178 (1978).

32. Desai, S.V., E.S. Daniel, and W.H. Corcoran, Rev. Sci., Inst., 39, 612 (1968).

33. Meubus, P., Can J. Ch. Eng., 52, 616 (1974).

34. Gold, D., J. of Phys., 10, 395 (1977).

35. Gouesbet, G., C.R. Acad. Sc. Paris, 280B, 597 (1975).

36. Gouesbet, G. and M. Trinite, Letters in Heat & Mass Transfer, 4, 141 (1977).

37. Lesinski, J., Gagné, R. and M.I. Boulos, 5th International Symposium on Plasma Chemistry, Edinburgh, U.K., August 10-14 2, 527 (1981).

38. Dundas, P.H., Induction plasma heating: measurement of gas concentrations, temperatures and stagnation heads in a binary plasma system. NASA CR-1527 (1970).

39. Eckert, H.U., J. Appl. Phys., 41, 1529 (1970).

40. Pridmore-Brown, D.C., J. Appl. Phys., 41, 3621 (1970).

41. Keefer, D.R., J.A. Sprouse and F.C. Lper, IEEE, Tran. Pl. Sc., PS-1, 71 (1973).

42. Eckert, H.U., Proceedings of the Internatinal Winter Conference, San Juan, Puerto Rico, Jan 7-11 (1980), Hyden Press, 35 (1981).

43. Eckert, H.U., 5th International Symposium on Plasma Chemistry, Edinburgh, U.K., 10-14 August, p. 781 (1981).

44. Aeschbach, F., "Computed electron density distribution in an inductively- coupled plasma discharge in Argon", ICP Informatin Newsletter, 6, 272-287 (1980).

45. Miller, R.J. and J.R. Ayen, J. Appl. Phys., 40, 5260 (1969).

46. Barnes, R.M. and R.G. Schleicher, Spectrochim. Acta, B30, 109 (1975).

47. Barnes, R.M. and S. Nikdel, Appl. Spectrosc., 29, 477 (1975).

48. Barnes, R.M. and S. Nikdel, J. Appl. Phys., 47, 3929 (1976).

49. Delettrez, J.A., "A numerical calculation of the flow and electrical characteristics of an argon induction discharge", Ph.D. Dissertatin, University of California, Davis (1974).

50. Boulos, M.I., IEEE, Trans. on Plasma Sc., PS-4, 28 (1976).

51. Boulos, M.I., R. Gagné and R.M. Barnes, C.J.Ch.E., 58, 367 (1980).

52. Gagné, R., "Etude de modélisation d'un plasma à induction généré à haute fréquence", M.Sc.A. Thesis, University of Sherbrooke, Québec (1970).

53. Mostaghimi, J., Proulx, P. and M.I. Boulos, J. Numerical H.T., 8, 187 (1985).

54. Mostaghimi, J., Proulx, P. and M.I. Boulos, J. Plasma Chemistry and Plasma Processing, 4, 129 (1984).

55. Patankar, S.V., "Numerical Heat Transfer and fluid flow", McGraw Hill, N.Y. (1980).

56. Genna, J.L., R.M. Barnes and C.O. Allemand, Anal. Chem., 49, 1450 (1977).

57. Boulos, M.I. and W.H. Gauvin, C.J.Ch.E., 52, 355 (1974).

58. Bhattacharya, D. and W.H. Gauvin, AIChEJ, 21, 879 (1975).

59. Gal-Or, B., J. of Eng. for Power, 102, 589 (1980).

60. Fiszdon, J.K., Int. J. Heat & Mass Transfer, 22, 749 (1979).

61. Vardelle, M., A. Vardelle, P. Fauchais and M.I. Boulos, AIChEJ, 29, 236 (1983).

62. Wei, D., S.M. Correa, D. Apelian and M. Paliwal, 6th International Symposium on Plasma Chemistry (ISPC-6), Montreal, 1, 83 (1983).

63. Boulos, M.I., IEEE, Trans. Pl. Sc., PS-6, 93 (1978).

64. Yoshida, T. and K. Akashi, J. Appl. Phys., 48, 2252 (1977).

65. Proulx, P., "Interactin plasma-particules dans la modélisation des plasmas à induction", mémoire de M.Sc.A., Université de Sherbrooke, avril (1984).

66. Proulx, P. J. Mostaghimi and M.I. Boulos, 6th International Symposium on Plasma Chemistry, Montreal, July (1983), 1, p 59 (1983).

67. Mostaghimi, J., Proulx, P., M.I. Boulos et R.M. Barnes, Sprectrochemical Acta, 40B, 153 (1985).

68. Proulx, P., Mostaghimi, J. and M.I. Boulos, "Plasma-particle interaction effects in induction plasma modelling under dense loading conditions", Int. J. Heat & Mass Transfer, in print (1985).

69. Bourdin, E., P. Fauchais and M.I. Boulos, Int. J. H. & M.T., 26, 567 (1983).

70. Xi Chen and E. Pfender, Plasma Chemistry and Plasma Processing, 2, 293 (1982).

71. Ibid, 2, 185 (1982).

72. Ibid, 3, 97 (1983).

73. Ibid, 3, 351 (1983).

74. Crowe, C.T., M.P. Sharma, D.E. Stock, J. Fluids Eng., 99, 325 (1977).

75. Mostaghimi, J., E. Pfender, Plasma Chemistry and Plasma Processing, 4, 199 (1984).

76. Reed, T.B., High Frequency floating review, 1, 6 (1961).

77. Donskoi, A.V., Dresvin, S.V., Voronin, K.K. and Volynets, F.K., Teplofiz. Vys. Temps. 3, 627 (1965).

78. Chase J. D. and Van Ruyven L.V., J. Crystal Growth, 5, 294 (1969).

79. Poole, J.W. and Vogel, Ch.E., NASA Contract Report, CR-1765 (1971).

80. Jurewicz, J., R. Kaczmarek and M.I. Boulos, ISPC-7, Eindhoven, July 1-5 (1985).

81. Johnson, D.L. and J.S. Kim, Mat. Sci. Monographs, Elsevier S. Pub. Co., 14, 573 (1982).

82. Kim, J.S., and D.L. Johnson, Ceramic Bull., 62, 620 (1983).

83. Johnson, D.L. and J.S. Kim, Mat. Sci. Monographs, Elsevier S. Pub. Co., 14, 573 (1982).

84. Nassau, K. and J.W. Shiever, Ceramic Bull, 54, 1004 (1975).

85. Rykalin, N.N., Pure & Appl. Chem., 48, 179 (1976).

86. Yoshida, T. and K. Akashi, Trnas. Japan Inst. of Metals, 22, 371 (1981).

87. Yoshida, T. . Endo., K. Saito, and K. Akashi, ISPC-6, Montreal, paper #A-7-3, July (1983).

88. Canteloup, J. and A. Mocellin, J. Special Ceramics, 6, 209 (1975).

89. J. Material Sci., Letters, 11, 2352 (1976).

90. Barnes, R.M., "Recent advances in emission spectroscopy", CRC Critical reviews, 203 (1978).

91. Thompson, M. and J.N. Walsh, "A handbook of inductively coupled plasma spectrometry", Blackie & Son Ltd. (1983).

92. Trassy, C. and J.M. Mermet, "Les applications analytiques des plasmas hf", Lavoisier, Paris (1984).

93. Boumans, P. Ed., "Analysis by Inductively Coupled Plasma Atomic Emission Spectrometry", J. Wiley, in print (1985).